2D and 3D Finite Element Analysis of Buffer-Backfill Interaction

Martino Leoni

Wesi Geotecnica Srl

August 2013

Tekijä(t) – Author(s)	Toimeksiantaja(t) – Commissioned by
Martino Leoni, Wesi Geotecnica Srl	Posiva Oy

Nimeke – Title

2D AND 3D FINITE ELEMENT ANALYSIS OF BUFFER-BACKFILL INTERACTION

Tiivistelmä – Abstract

Methods for backfilling and sealing of disposal tunnels in an underground repository for spent nuclear fuel are studied in cooperation between Finland (Posiva Oy) and Sweden (Svensk Kärnbränslehantering AB, SKB) in "BAckfilling and CLOsure of the deep repository" (Baclo) programme. Baclo phase III included modelling task force SP1: Finite element modelling of deformation of the backfill due to swelling of the buffer. The objective of the finite element modelling of the backfill was to study the interaction between the buffer and backfilling. The calculations aimed to find out how large deformations can happen in the buffer-backfill interface causing loosening of the buffer bentonite above the canister. The criterion used was that the saturated density of the buffer right above the canister should be higher than 1990 kg/m^3. This report presents the results of finite element numerical analyses carried out by Wesi Geotecnica Srl.

The modelling calculations were conducted with the so-called OL1-2 deposition tunnel geometry (Juvankoski 2009). Several parameters have been considered, varying from geometry variations to different mechanical constitutive models for different components of the model. In all analyses it has been assumed that the buffer material is fully saturated, thus exerting the isotropic swelling pressure estimated in the range 7 MPa ó 15 MPa, against a fully-dry backfill, which is no doubt the "worst case scenario" with the highest risk to lead in decrease in dry density of the buffer. Friedland clay has been considered for backfill blocks and 30/70 mixture for foundation bed on which backfill blocks are installed.

Preliminarily, finite element analyses have been performed with newly released PLAXIS 2D 2010 within the assumption of axial symmetry, the purpose of this first set of calculations being the evaluation of most relevant parameters influencing the deformations of buffer material. Hence, full 3D calculations have been performed with PLAXIS 3D 2010/2011, aiming to a realistic estimation of buffer deformation. In this latter set of finite element analyses, interface behaviour between block modules has been simulated by explicit use of PLAXIS interface elements. Whenever possible, model symmetry has been exploited in order to reduce the degrees of freedom of the analysis.

Globally, FE analyses showed a good response of the buffer-backfill system, thus ensuring that the denisty of buffer material is not dropping below the threshold value of 1990 kg/m^3. Such value is the one considered necessary to ensure the effectiveness and durability of the buffer (Hansen *et al.* 2009). Furthermore, the results enabled to identify what are the most relevant components of the system in the light of reducing the heave at the top surface of buffer.

Tekijä(t) – Author(s)

Martino Leoni, Wesi Geotecnica Srl

Toimeksiantaja(t) – Commissioned by

Posiva Oy

Nimeke – Title

PUSKURIN JA TÄYTÖN VÄLISEN VUOROVAIKUTUKSEN NUMEERINEN MALLINNUS

Tiivistelmä – Abstract

Posiva on tutkinut menetelmiä loppusijoitustunnelin täyttämiseksi ja sulkemiseksi käytetyn ydin-polttoaineen loppusijoitustilassa yhteistyössä SKB:n (Svensk Kärnbränslehantering AB) kanssa ns. Baclo-ohjelmassa (Baclo = BAckfilling and CLOsure of the deep repository). Baclo-ohjelman kolmannessa vaiheessa, työpaketissa 1, tutkittiin elementtimenetelmän avulla (FEM) täytön defor-maatiota puskurin paisumisen seurauksena. Laskelmilla pyrittiin selvittämään kuinka suuria defor-maatioita voi tapahtua puskurin ja täytön rajapinnalla ja johtaisivatko ne puskuribentoniitin löyhtymiseen kapselin yläpuolisessa tilavuudessa. Puskurin tiheyden kriteerinä käytettiin saturoi-tunutta tiheyttä >19,5 kN/m^3. Tässä raportissa esitetään elementtimenetelmällä tehtyjen numee-risten analyysien tulokset. Analyysit suoritti Wesi Geotecnica Srl.

Analyyseissä käytettiin loppusijoitustunnelien OL1-2 geometriaa (Juvankoski 2009). Mallinnuk-sessa selvitettiin useiden parametrien vaikutusta, vaihdellen tunnelin geometriasta eri kom-ponenteille käytettävään konstitutiiviseen malliin. Kaikissa analyyseissä oletettiin, että puskuri-materiaali on täysin kyllästyneessä tilassa aiheuttaen vaihteluväliltään 7-15 MPa paineen täysin kuivaa täyttöä vasten. Tämä edustaa ns. pahinta mahdollista skenaariota, jolla on suurin riski johtaa puskurin kuivatiheyden laskemiseen. Täyteainelohkoina tarkasteltiin Frieldland-sav-loh-koja ja lattiantasauskerroksen materiaalina bentoniitin ja murskeen seosta (30:70), jonka päälle lohkot ladotaan.

Elementtianalyysit tehtiin pääasiassa 2010 julkaistulla PLAXIS 2D versiolla käyttäen hyväksi mallin aksiaalista symmetriaa. Ensimmäisten laskelmien tarkoituksena oli määritellä parametrit, joilla on eniten vaikutusta puskurimateriaalin deformaatioon. Tämän jälkeen suoritettiin PLAXIS 3D 2010/2011 -versiolla laskelmia, joilla pyrittiin puskurin deformaation realistiseen arvioon. Näissä jälkimmäisissä elementtianalyyseissä lohkomoduulien väliset rajapinnat kuvattiin käyttäen PLAXIS-rajapintaelementtejä. Milloin mahdollista, mallin symmetrisyyttä on hyödynnetty ja käytetty vain puolikasta mallia laskennan keventämiseksi.

Yleisesti ottaen analyysit osoittivat puskurin ja täytön muodostaman kokonaisuuden toimivan tavoitellulla tavalla siten, ettei puskurimateriaalin tiheys ei laske alle vaatimusrajan 19.5 kN/m^3. Tätä raja-arvoa pidetään tarpeellisena puskurin toimintakyvyn takaamiseksi (Hansen et al. 2009). Edelleen, tulokset mahdollistivat systeemin tärkeimpien komponenttien identifioimisen koskien sitä miten puskurin yläosan nousua sijoitustunnelin täytteeseen voidaan vähentää.

TABLE OF CONTENTS

PREFACE

Posiva Oy (Posiva) and Swedish Nuclear Waste Management Company (SKB) coordinate the 4 phase programme of "BAckfilling and CLOsure of the deep repository" (Baclo). Baclo phase III includes modelling task force SP1: Finite element modelling of the swelling of the buffer against backfill in the deposition tunnel, functional studies. The objective of the first finite element modelling of the backfill was to find out the interaction of the buffer and backfilling (Börgesson & Hernelind 2009; Korkiala-Tanttu 2009). The stress – deformations distribution in this interaction area was studied to find out the most critical design cases and problems.

Recently, Posiva has appointed Wesi Geotecnica Srl (Wesi) to perform a further series of finite element analyses of buffer-backfill interaction in the light of the knowledge on geometry and materials gained since previous analyses (Börgesson & Hernelind 2009; Korkiala-Tanttu 2009). The purpose of this further series of numerical analyses is to take into account plasticity, interfaces and aspects not included in previous analyses due to limited computational power available. Furthermore, recent development of PLAXIS finite element program enabled a significant improvement in the numerical models.
The present document presents the results obtained with the numerical analyses carried out by Wesi, with particular focus on the fulfilment of design requirements for buffer material.

The work was carried out by Martino Leoni (Wesi). Leena Korkiala-Tanttu (Aalto University), Paula Keto, Xavier Pintado, Elisa Rautioaho and Jorma Autio (B+Tech), Kari Koskinen, Petri Koho and Johanna Hansen (Posiva) participated in several management meetings in which mechanical properties, geometry, procedures and results obtained have been discussed.

Massa (Italy), June 2011, Wesi Geotecnica Srl

1   BACKGROUND

One essential functional requirement for the deposition tunnel is that the backfill as a whole has a sufficient rigidity in unsaturated state to ensure that, even if the buffer is swelling and compressing the backfill, the buffer density does not decrease below a critical value estimated in 1990 kg/m^3 (Hansen *et al.* 2009). Such limiting value can be regarded as minimum admissible value in the buffer region between canister top and foundation floor, so that the buffer material keeps a sufficiently low permeability value to enable it to stop contaminated fluid in the unlikely event of leaking from the canister. The stress and displacement balance in the surface of the buffer depend on the saturation degree of the buffer and backfill. However, in the analyses the most critical situation of fully saturated buffer (thus exerting the maximum swelling pressure against backfill) and completely dry backfill (thus opposing the minimum resistance against buffer swelling) has been considered. In that sense, the results can be considered on the safe side with respect to expected swelling of buffer blocks.

2 OBJECTIVES OF THE MODELLING TASKS

Although the main requirement is the development of a maximum swelling within the threshold value indicated in Section 0, there are several issues for which numerical analysis should enable to gain insight. As argued, the global requirement on the backfill is to provide favourable conditions for buffer and canister, and the requisites can be summarized as follows: 1) the backfill shall limit advective flow along the deposition tunnels, 2) the chemical composition of the backfill shall not jeopardise the performance of the buffer, canister or bedrock, 3) the backfill shall keep the buffer in place and 4) the backfill shall contribute to the mechanical stability of the deposition tunnels. Of all the implications connected with this requirement, the only aspect that is focused on in present analyses is the ability of backfill to keep buffer in place and to ensure that its deformations are acceptable.

Another important factor is the swelling pressure, in this work estimated in the range 7 MPa ó 15 MPa, which on one hand contributes to the sealing of canister, but on the other hand might be the cause of excessive loss of density. Studies recently presented by Karnland *et al*. (Karnland *et al.* 2006; Karnland 2010) show that the expected swelling should not exceed 11 MPa. However, the conservative value of 15 MPa was herein chosen as upper bound.

Factors such as leakage of harmful material from the host rock or damage of hydraulic or mechanical properties of buffer/backfill system due to mass transport through flow channels before a fully saturated state is reached are beyond the scope of this set of present work.

Furthermore, the effectiveness of buffer/backfill system depends upon the global system rigidity, and therefore the stiffness of its single components and their mutual interfaces. Strength and stiffness parameters of components such as blocks, 30/70 mixture used in foundation bed, pellets between block assembly and host rock have been widely investigated (Korkiala-Tanttu *et al.* 2007; Börgesson & Hernelind 2009; Korkiala-Tanttu 2009; Johannesson *et al.* 2010) and could be determined from laboratory tests results. On the other hand, interface behaviour has not been investigated thoroughly and for this reason a series of laboratory tests has been planned for the future. As long as new test data are not available, mechanical parameters (strength and stiffness) has been estimated on the basis of a few tests available, e.g. (Kuula-Väisänen *et al.* 2009).

3   DESCRIPTION OF THE MODELLING METHOD

The geometry of the problem is described in Juvankoski (2009) and it is the reference solution adopted for Olkiluoto deposition hole, canister and buffer (Figure 1). Several different geometries accounting for slight differences that can be found on site are taken into account, as indicated in Section 4 and according to Hansen *et al.* (2009).
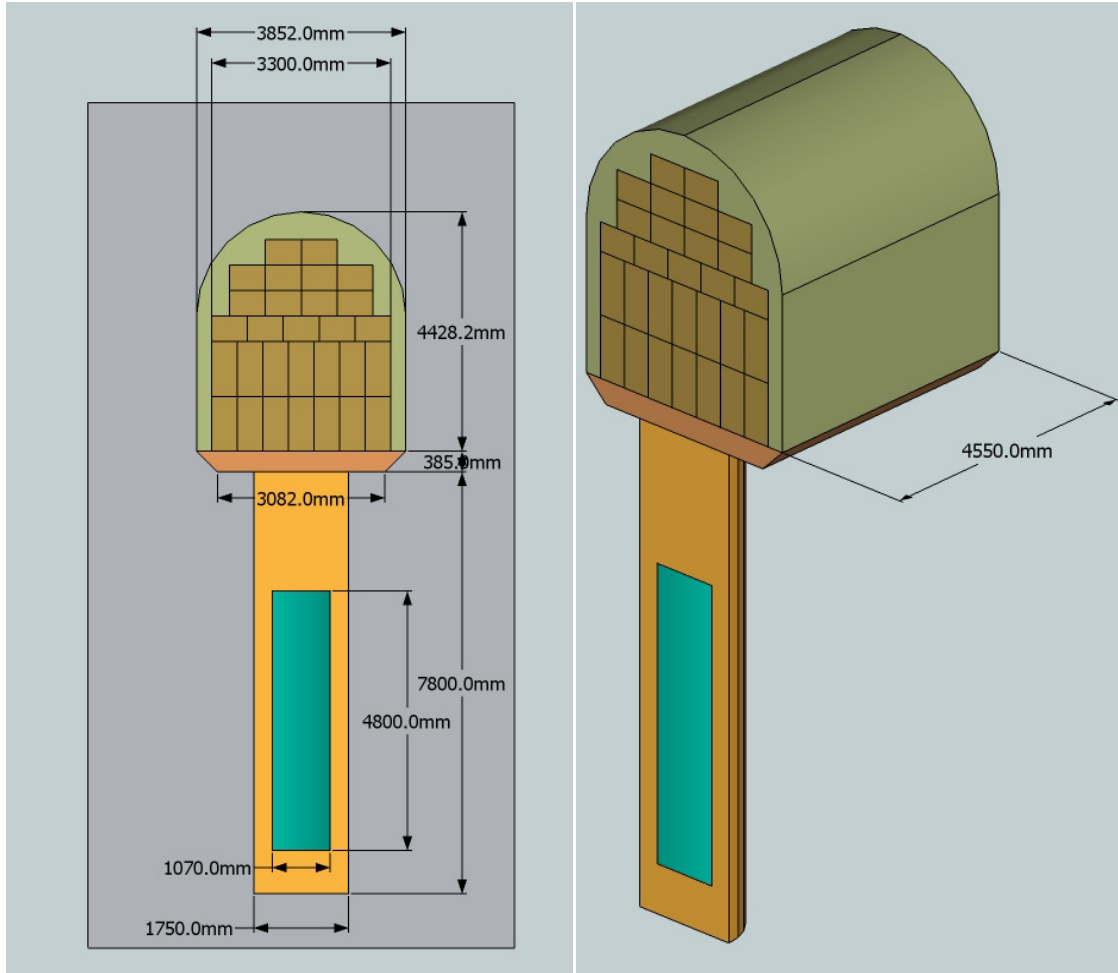

Figure 1. Geometry of OL1-2 section. (Right: host rock excluded from visualization).

As preliminary study, a series of finite element analyses in the assumption of axial symmetry has been carried out. A cross section has therefore been modelled in commercial FE code PLAXIS 2D 2010/2011. Clearly the results obtained are not assumed to be realistic as the hypothesis of axial symmetry holds for the deposition hole but it is inappropriate for backfill region. However, being the scope of this first set of analysis the calibration of relevant parameters, axial symmetric analyses are perfectly suited to the purpose. All the results obtained from the preliminary set of analyses is reported in Appendix 1, with the exception of a single case where the whole height of buffer section was taken into account, which is included in the main Section of this report.

Analyses including the full 3D geometry have been therefore performed. Geometry of the standard case is shown in Figure 1. Backfill block modules have been modelled as discrete blocks system, each block surrounded by elastic perfectly-plastic interfaces.

Buffer bentonite has been assumed in fully saturated state, backfill in dry state (no increase in water content occurred after installation). This is in favor of safety, as backfill swelling due to saturation would prevent the penetration of saturated buffer.

Several geometry and mechanical variations have been considered with the purpose of performing a parametric study on a wide range of aspects. In the main series of calculations (3D04_II-III, 3D08_II-III, see Table 2), where the most advanced set of constitutive models has been chosen, the results should be regarded also under the quantitative point of view.

4   FINITE ELEMENT MODEL

Two series of finite element analyses have been performed: a first preliminary axisymmetric series (prefix AX in Table 2) aiming to identify the most relevant factors influencing the expansion of the buffer material into the backfill, followed by a second set of analyses including the full 3D geometry and interface elements between the blocks (prefix 3D in Table 2). The latter series has been focused on a narrowed set of variables considered as most relevant from preliminary axisymmetric analyses.

The finite element mesh for first axisymmetric calculation is shown in Figure 2. 2600 6-noded elements have been used, with 5700 nodes and an average element size of about 130 mm. Horizontal and vertical displacements have been prevented at the sides and bottom of the mesh, respectively.

The process of saturation and swelling of buffer material is simulated by a precompressed state achieved by applying distributed loads on outer surface followed by stress release and subsequent expansion in deposition hole. Considering that the hydraulic process of saturation has been completely simulated by means of mechanical forces, water pressure has not been introduced in the model.

Being the host rock modelled as very stiff linear elastic material, it is not expected to undergo significant deformations and therefore the host rock should be regarded as a mechanical boundary condition to the deforming buffer-backfill system.

To model the interaction, interfaces have been used in every contact region between different materials. Due to the assumption of axial symmetry, no interfaces have been used for block-block contact, and the region occupied by block has been modelled as a continuum. Explicit use of interfaces has been made in full 3D analyses, as shown in next Section.

As for initial conditions, the host rock has been assumed to be isotropic, hence $K_{0x} = K_{0y} = 1$, although specific studies could show initial stress anisotropy. However, since the focus is on buffer-backfill system, initial stress state in the rock mass is not relevant for this study. Buffer blocks, foundation bed, blocks and pellets were installed after simulating the excavation of deposition tunnel and deposition hole in the rock mass. A more detailed description of initialization of the model is given in Section 4.4.

After verifying that deformations are mainly concentrated in the buffer part above canister top, axisymmetric analyses AX02-09 reported in Appendix 1 have been performed with a simplified model including only the top half of the canister. This in order to reduce the calculation time without spoiling the accuracy required for this set of analyses preparatory to 3D modelling.
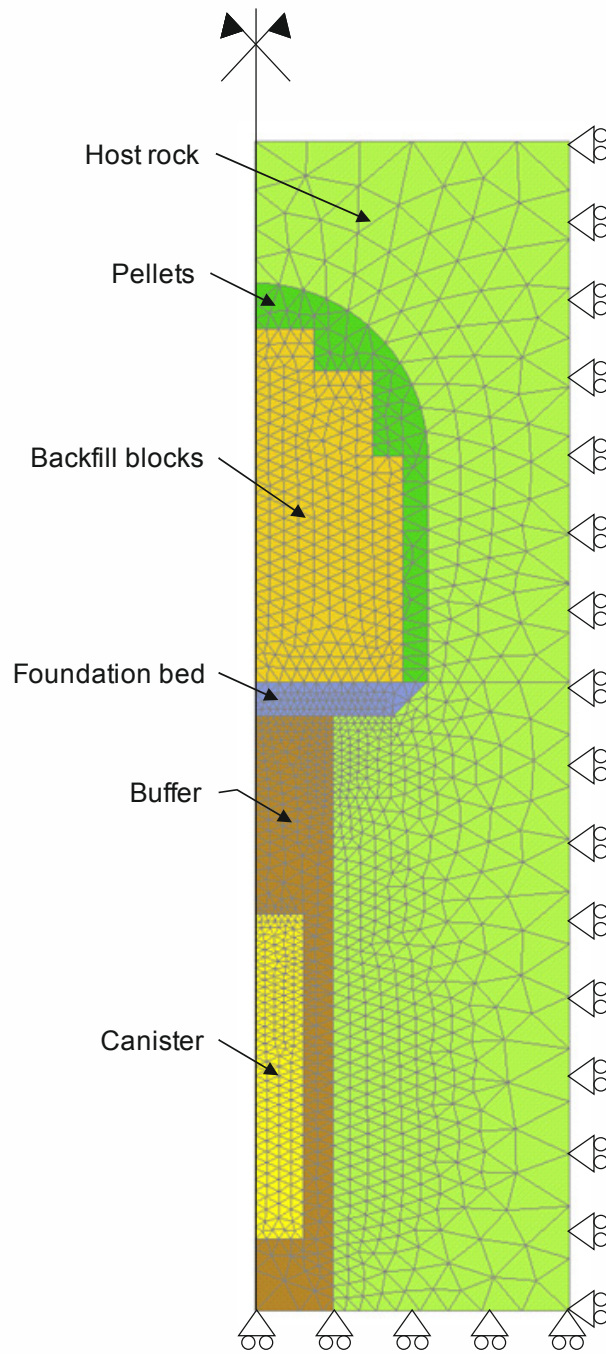
Host rock

Pellets

Backfill blocks

Foundation bed

Buffer

Canister

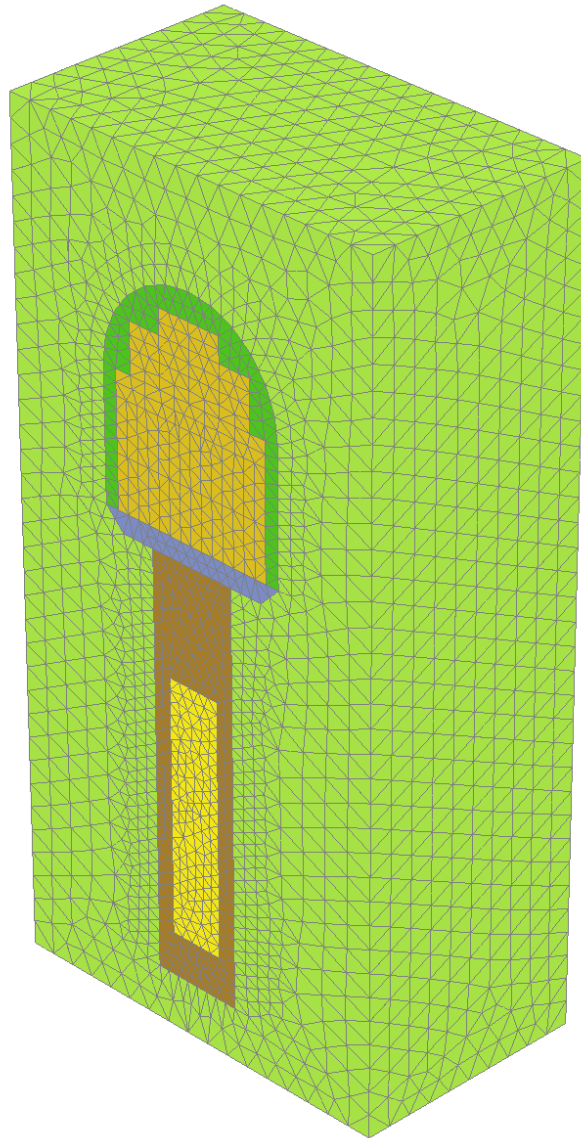**Figure 2.** *Mesh for axisymmetric calculations, case AX-01.*

Figure 3. *Mesh for 3D calculations, case 3D-04.*

The typical finite element mesh for 3D calculations is shown in Figure 3. 92 000 10-noded elements have been used, with 160 000 nodes and an average element size of about 80 mm. Due to the high density of finite elements in the plastic zones a mesh sensitivity analysis was considered unnecessary. Interfaces have been inserted in every contact region between different materials. With the exception of preliminary analyses performed with the purpose of setting-up the appropriate element size and constitutive models (3D01 and 3D02, see Table 2), interfaces have been used at the block-block contact. For symmetry reasons, it was possible to simplify the model considering only one half of the section between two contiguous deposition holes. Whenever interfaces were not included, symmetry conditions enabled the modelling of only one quarter of the whole region. In Case 3D08 (Table 2), where the blocks are overlapping also in longitudinal direction, the whole region needed to be included in the FE model.
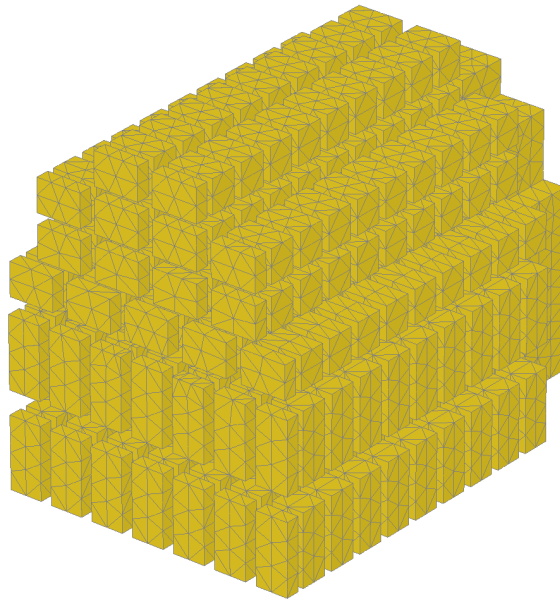
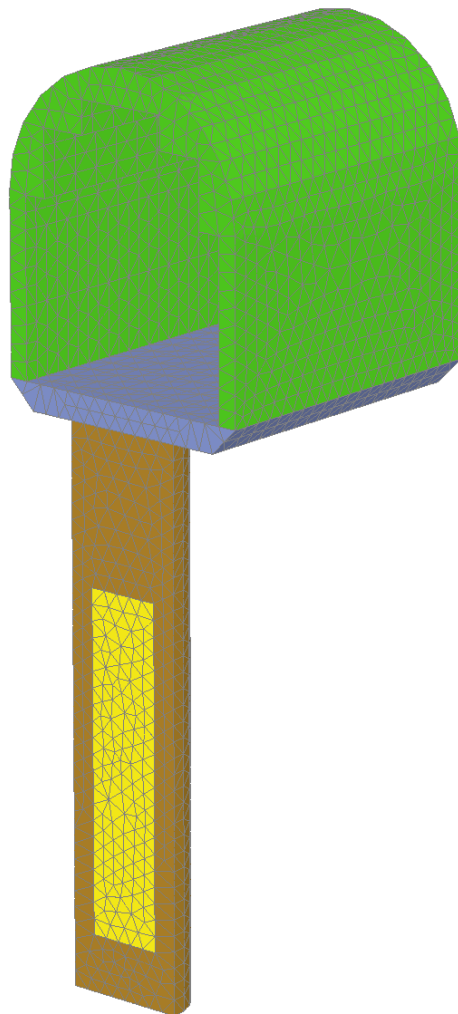**Figure 4.** *Exploded view of backfill blocks.*

Figure 5. *Pellets (green), foundation bed (purple), buffer (brown) and canister (yellow).*

The assembly of non-overlapping blocks is shown in an exploded view in Figure 4. Blocks are not overlapping in the longitudinal direction, whereas one can clearly see that the third and fourth block layers are overlapping in the cross section. Blocks are assembled in modules of eight each, with a module size of 471.4 x 1014.2 x 400 mm (Hansen *et al.* 2009). Pellet region between blocks and host rock floor and foundation bed on which block modules are placed are shown in Figure 5, along with the half cylinder of buffer material and canister.

In order to evaluate the influence of various parameters which may vary during design and construction phases, a parametric study has been carried out. Details on the variables involved in the parametric study are described in the following Sections:

- Constitutive models (CM)

In a deformation problem the choice of the proper constitutive model is of great importance. On the other hand, the use of advanced models implies the availability of accurate test results to identify the constitutive parameters and an increase of the complexity of the problem. Therefore, the use of advanced constitutive law has been narrowed down to the most relevant materials where deformations are most likely to concentrate. The double-hardening Hardening Soil model (see Section 4.2.1) has been chosen for the foundation bed and sprayed pellets between the backfill blocks and the deposition tunnel roof. Furthermore, a simple elastic model with stress-dependent stiffness (poroelasticity, Section 4.2.3) was implemented and used for some selected analyses. Linear elasticity is assumed for the blocks, for the expanding saturated buffer blocks, canister and surrounding rock. However, since plastic deformations are supposed to develop at the interface between materials, each interface has been explicitly introduced in the model by assuming a linear elastic – perfectly plastic behaviour based on Mohr-Coulomb failure criterion (see Section 4.2.2). A full description of theoretical background of the constitutive models used in the analysis is given in Section 4.2.

As for the combinations considered in finite element analyses, in the basic one (CM-1) linear elasticity has been applied to all materials. Furthermore, Hardening soil model has been applied to foundation material (standard case CM-2) and to both foundation and pellets (CM-3). An additional analysis with linear elastic foundation bed reproducing the stiffness of pellets instead of 30/70 mixture has been performed (CM-4). In the last combination considered (CM-5) poroelasticity was used for saturated buffer blocks. The details of parameter combinations are summarized in Table 1.

A detailed description of constitutive parameters for each constitutive model is given in Table 4, and in Appendix 2 is reported an overview of the sources from which the parameters have been identified.

Table 1. Combinations of constitutive model for model parts.

Analysis type	Foundation Bed	Buffer	Pellets
CM-1	Linear Elastic (LE)	Linear Elastic (LE)	Linear Elastic (LE)
CM-2	Hardening Soil (HS)	Linear Elastic (LE)	Linear Elastic (LE)
CM-3	Hardening Soil (HS)	Linear Elastic (LE)	Hardening Soil (HS)
CM-4	Bent.pellets (LE)	Linear Elastic (LE)	Linear Elastic (LE)
CM-5	Hardening Soil (HS)	Poroelastic (PE)	Linear Elastic (LE)

- Over-excavation (OE)

Due to the tunnel excavation technique (drill and blast) a certain degree of drifting from the dimensions of theoretical tunnel section is expected, thus influencing the thickness of bentonite pellets layer between blocks and surrounding rock and the thickness of foundation bed. Various possible geometries have been taken into account in axisymmetric analyses, including three different over-excavation values (20 % (standard case), OE-1 10 %, OE-2 36 %) and a case with 550 mm of foundation floor and 10 % over-excavation (OE-3). The cases considered in the analyses are shown in Figure 6.

- Roof gap (RG)

The blocks will be emplaced in deposition tunnel so that the empty space is between the top of the stack and the host rock is 100 mm minimum. The empty spaces will be backfilled with sprayed bentonite pellets. Due to the roughness of rock face it is likely that the blocks-rock gap is not perfectly sealed by sprayed pellets before full saturation of backfill. Specific analyses have been carried out to check the effect on the deformability of the system. The gap has been simulated by reducing to very low value the pellet-roof interface stiffness, by assuming that the resulting deformation is not exceeding the estimated gap size. It is worth noting that, considering the way interface mechanical behaviour is formulated in PLAXIS, by reducing the stiffness to zero the thickness of the interface itself becomes non-relevant to its mechanical behaviour. In case the resulting displacement exceeds the size of the physical gap, whilst in reality the gap would be sealed thus becoming less compressible, in PLAXIS it will be still count as a gap as no contact algorithm is implemented in the program.

- Chamfer (CH)

The intersection between deposition hole and deposition tunnel will be shaped in such a way that it can ease the insertion of the canister. The shape of this so-called chamfer has been varied in 3D analyses from cylindrical (CH-1) to a wedge (CH-2) keeping constant width and depth of OL1-2 deposition hole given in Appendix 1 in Juvankoski (2009).

- Block assembly (BA)

Two different backfill blocks assemblies are considered, without (BA-1) and with overlapping (BA-2) between blocks across contiguous vertical layers. The purpose is to investigate on the effect that block assembly can have on the backfill resistance to buffer swelling. Unless differently stated, the block region treated as continuum.
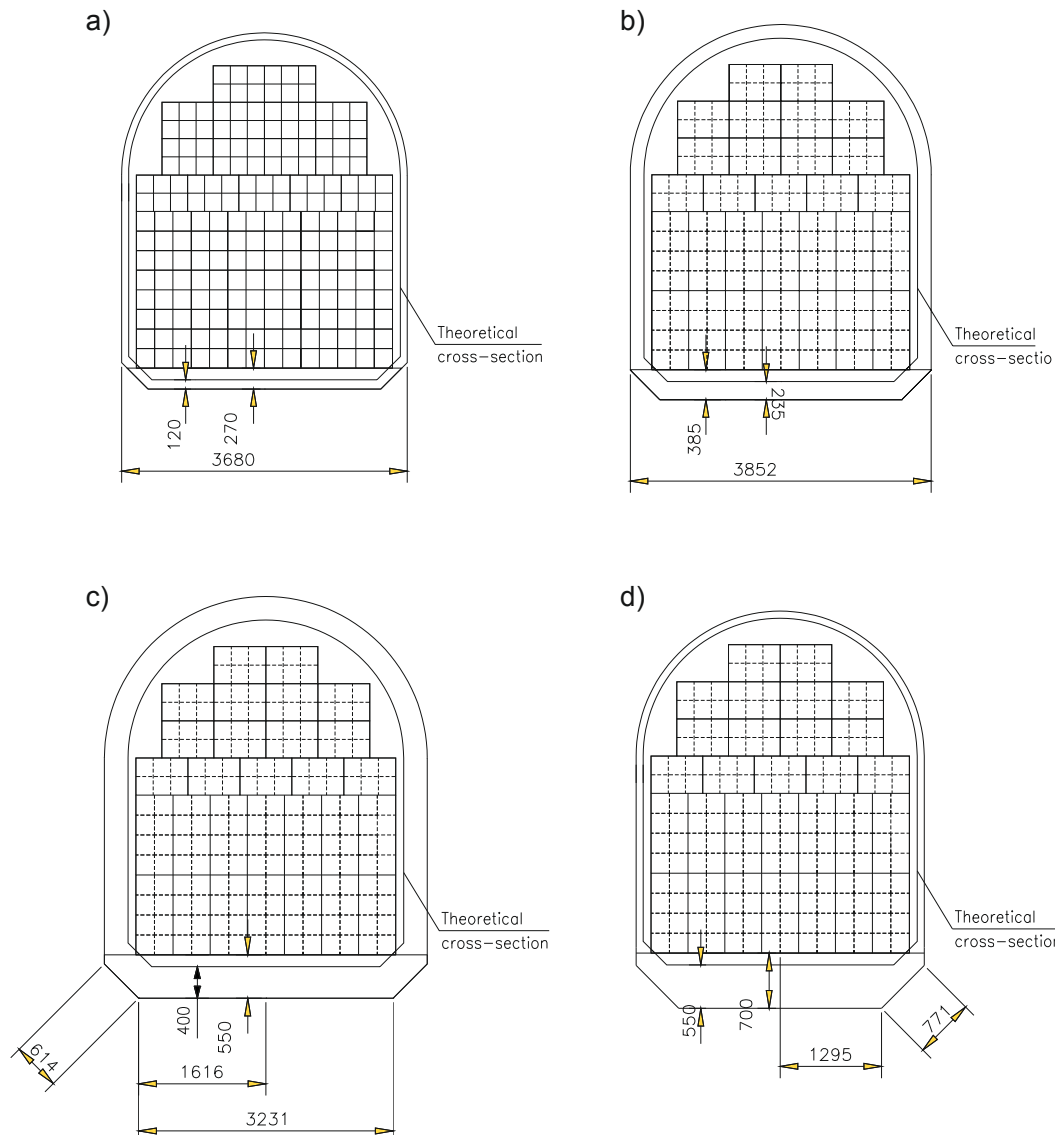
Figure 6. Deposition tunnel sections a) OE-1 b) standard (20 %) c) OE-2 d) OE-3.

- Load application

In a preliminary set of analyses a distributed load of 7 MPa was applied to the interface between buffer and foundation bed, with the purpose of simulating the expansion of the buffer into backfill due to saturation of buffer blocks. This in analogy with the approach described in Korkiala-Tanttu (2009). In addition, in 2D analyses, the uniformly distributed load of 7 MPa was applied one buffer block (400 mm) above canister top and one block below. As result of preliminary analyses, it has been agreed that the assumption of a uniform swelling pressure of 7 MPa is not realistic, therefore in all analyses herein presented the buffer material has been precompressed to an isotropic stress of 7 MPa and then its expansion simulated by removing the prestress previously applied by means of distributed loads. Contact pressure at the buffer-foundation interface is the result of such expansion and, as shown in Section 4, never exceeds the value of about 3 MPa. Due to the above considerations, the results of preliminary test have been excluded from this report.

The whole set of analyses performed is summarized in Table 2.

Table 2. *Finite element analyses. In gray shading standard case 3D04.*

Analysis type	Constitutive Model	Over-excavation	Roof Gap	Chamfer	Block Assembly	Load (MPa)
AX01	CM-2					7
AX02 (Appendix1)	CM-1					7
AX03 (Appendix1)	CM-2					7
AX04 (Appendix1)	CM-4					7
AX05 (Appendix1)	CM-2	OE-2				7
AX06 (Appendix1)	CM-2	OE-1				7
AX07 (Appendix1)	CM-2	OE-3				7
AX08 (Appendix1)	CM-2		RG			7
AX09 (Appendix1)	CM-2			CH-1		7
3D01	CM-1					7
3D02	CM-2					7
3D03	CM-3				BA-1	7
3D04	CM-2				BA-1	7
3D04_II	CM-5				BA-1	7
3D04_III	CM-5				BA-1	15
3D05	CM-2		RG		BA-1	7
3D06	CM-2			CH-1	BA-1	7
3D07	CM-2			CH-2	BA-1	7
3D08	CM-2				BA-2	7
3D08_II	CM-5				BA-2	7
3D08_III	CM-5				BA-2	15
3D09	CM-2				BA-1	15

Results of analyses performed using poroelastic constitutive model should be regarded as the reference ones. Unfortunately, due to the fact that the use of user defined models in PLAXIS with a high number of elements causes an enormous increase of calculation time, it was decided to limit the analysis with poroelasticity to two standard cases (3D04 and 3D08, non-staggered and staggered blocks, respectively) with swelling pressures of 7 MPa and 15 MPa (subcases II and III).

4.1 Interface elements

The interface elements follow Mohr-Coulomb constitutive behaviour as described in Figure 7 for a constant normal stress. The parameters for the interface Mohr-Coulomb constitutive model are c_{in}, φ_{in}, ψ_{in}, ν_{in} and E_{in}, which are the interface cohesion, friction angle, dilatancy angle, Poisson's ratio and elastic stiffness respectively. Another important parameter for the interface element is the virtual interface thickness t_{in}. As for the interface stiffness, it can be specified as a linear elastic stiffness or non-linear elastic stiffness. Due to the lack of specific tests needed to calibrate interface behaviour, in this case a simple linear elastic constitutive law has been chosen.

As for the interface thickness t_{in}, the PLAXIS program applies the default value of 0.1 times the average element size of the elements in the model. However, in the 2D program it can be specified independently, whereas in the 3D PLAXIS the default value cannot be set to a different one by the user.
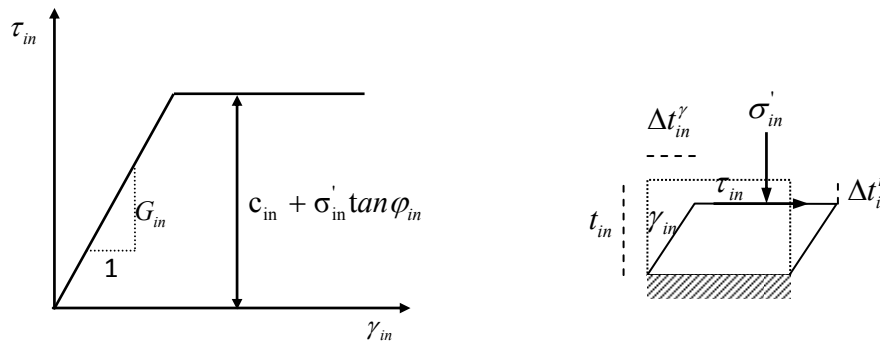

Figure 7. *(L) Shear stress and shear strain relationship for interface at constant normal stress (R) The interface deformation mechanism.*

4.2 Material models and constitutive parameters

4.2.1 The Hardening-Soil model

In the analyses bentonite pellets and foundation material were modelled with the Hardening-Soil Model which is a double hardening model. By introducing two more yield surfaces next to the Mohr-Coulomb failure criterion, both irreversible plastic shear strains due to primary deviatoric loading as well as irreversible volumetric strains due to primary isotropic loading can be described by the model. Further model features are stress dependent stiffness and the distinction between primary loading and unloading or reloading. The material parameters of the Hardening-Soil model are shown in Table 3. In the following, the meaning and determination of these parameters from laboratory tests is explained in more detail.

Meaning of the parameters:

a)   Strength parameters and dilatancy angle (φ', c', $\sigma_{Tension}$, ψ)

The parameters φ' and c', correspond to the shear strength parameters according to Mohr-Coulomb (see Figure 8). They can be determined from triaxial or shear test data.

In absence of laboratory test data, they can be correlated to in-situ test data. Material softening often observed in dense soils is not accounted for in the Hardening-Soil model.

Table 3. *Required parameters of the Hardening-Soil model.*

| Parameter		Explanation
γ	[kN/m³]	Unit weight (unsaturated)
γ_r	[kN/m³]	Unit weight (saturated)
φ'	[°]	Friction angle (Mohr-Coulomb)
c'	[kPa]	Cohesion (Mohr-Coulomb)
ψ	[°]	Angle of dilatancy
ν_{ur}	[-]	Poisson's ratio unloading-reloading
E_{50}^{ref}	[kPa]	Secant modulus for primary triaxial loading
E_{oed}^{ref}	[kPa]	Tangent modulus for oedometric loading
E_{ur}^{ref}	[kPa]	Secant modulus for un- and reloading
m	[-]	Exponent of the Ohde/Janbu law
p^{ref}	[kPa]	Reference stress for the stiffness parameters
K_0^{nc}	[-]	Coefficient of earth pressure at rest (NC)
R_f	[-]	Failure ratio
$\sigma_{Tension}$	[kPa]	Tensile strength
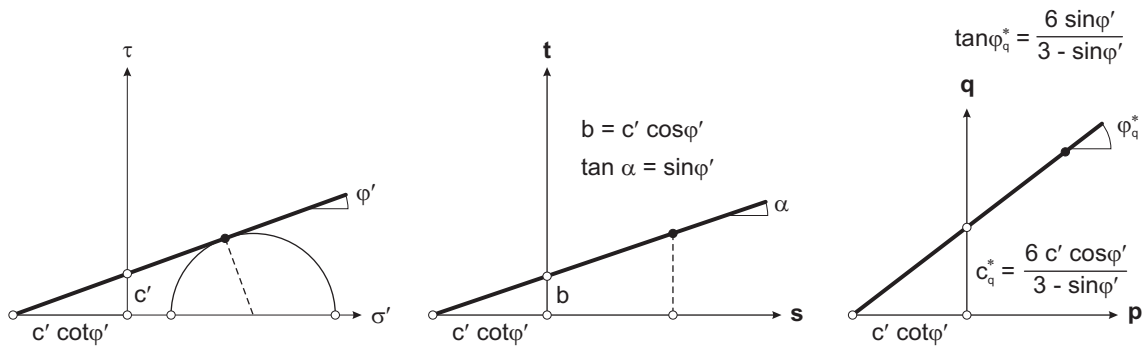
Figure 8. *Different ways of visualizing the Mohr-Coulomb criterion.*
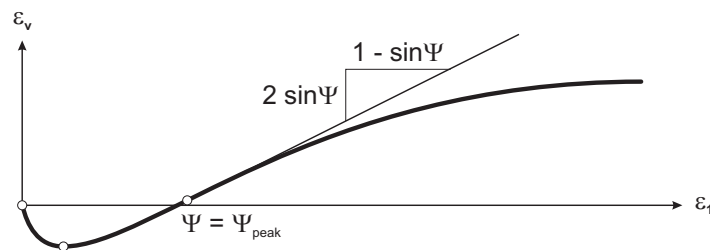

Figure 9. *Determination of ψ in a drained, triaxial test.*

The parameter $\sigma_{Tension}$ describes the maximum tensile strength of the material, and to control its maximum allowable value the constitutive model introduces a further yield surface (Tension Cut-Off surface, TCO) otherwise defined by the maximum value of c'cotφ'.

The dilatancy angle ψ describes the volumetric behaviour of the soil under deviatoric loading. In simple shear ψ corresponds to the angle of the deviation of the grain movement to the direction of shearing. In a triaxial test the dilatancy angle can be determined as shown in Figure 9.

b)   Stiffness parameters (ν_{ur}, E_{ur}^{ref}, E_{50}^{ref}, E_{oed}^{ref}, m, p^{ref}, R_f)

The elastic stiffness matrix of the Hardening-Soil model is quantified using the parameters ν_{ur} and E_{ur}^{ref}. If no plastic straining occurs (stresses inside the yield surfaces) these elastic parameters identify, in combination with the parameter m, the stress strain behaviour of the model. The elastic Poisson's ratio ν_{ur} and the elastic stiffness E_{ur}^{ref} can be determined in a triaxial test. The secant stiffness E_{ur}^{ref} is determined in a un-/reloading loop (see Figure 10).

The index „ref" indicates, that the elasticity modulus E_{ur}^{ref} as well as the stiffness parameters E_{50}^{ref} and E_{oed}^{ref} introduced below, relate to a reference stress p_{ref}. According to the assumption of Ohde (1939) for unloading-reloading stiffness, these parameters are converted to the present stress as follows:

$$E_{ur} = E_{ur}^{ref}\left(\frac{\sigma_3 + c\cot\varphi'}{p_{ref} + c\cot\varphi'}\right)^m , \quad E_{50} = E_{50}^{ref}\left(\frac{\sigma_3 + c\cot\varphi'}{p_{ref} + c\cot\varphi'}\right)^m \quad \text{and} \quad E_{oed} = E_{oed}^{ref}\left(\frac{\sigma_1 + c\cot\varphi'}{p_{ref} + c\cot\varphi'}\right)^m$$
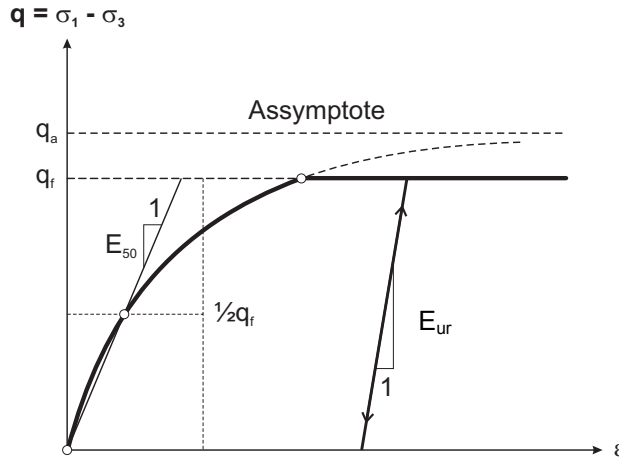

Figure 10. *Determination of E_{ur} and E_{50} in a drained triaxial test with a deviatoric failure stress q_f.*

E_{50}^{ref} indicates the secant modulus in primary triaxial loading when reaching half the ultimate deviatoric stress q_f (see Figure 10) and E_{oed}^{ref} the tangent modulus in an oedometer test for primary axial load of σ_1 = pref.

The ratio of q_f and q_a is given by the failure ratio R_f (see Figure 10), where the ultimate deviatoric stress q_f is defined by the shear strength parameters φ' and c'. When assuming $R_f = 1.0$ an asymptotic approach of the stress strain curve to the ultimate deviatoric stress ($q_f = q_a$) is given. Smaller values of R_f yield non-asymptotic stress strain curves, similar to the one shown in Figure 10. However, $R_f < 1.0$ often produces more accurate model predictions, i.e. better agreement with test data.

c)   Miscellaneous (γ, γ_r, K_0^{nc})

The unit weights γ and γ_r define the unsaturated and the saturated weight of the material, respectively. The coefficient of earth pressure at rest K_0^{nc} identifies the horizontal stress for normally consolidated soils. The rate of plastic-deviatoric strains in a compression test (steepness of the cap) in the Hardening-Soil model is calculated based on K_0^{nc}.

4.2.2 The Mohr-Coulomb model

Strength parameters and dilatancy of the model, including TCO surface, have been introduced in Section 4.2.1 and the description is not repeated here. In the present Section it is focused on stiffness parameters, which are particularly relevant in the model provided that no hardening surface is defined and that plastic (irrecoverable) strains are generated only when the stress state reaches Mohr-Coulomb failure envelope.

a)   Stiffness parameters (ν', E_{ref})

For rock mass, canister, backfill and buffer blocks have been assumed isotropic elastic, therefore Young's modulus E_{ref} and Poisson's ratio ν' are needed for full description of deformability of rock mass assumed as a continuum.

b)   Miscellaneous (γ, γ_r, K_0^{nc})

The unit weights γ and γ_r define the unsaturated and the saturated weight of the material, respectively. The coefficient of earth pressure at rest K_0^{nc} identifies the horizontal stress for normally consolidated soils, and in Mohr-Coulomb model the horizontal earth pressure at rest is defined by default in terms of Poisson's ratio as $K_0^{nc} = \nu' / (1 - \nu')$. However, in PLAXIS the default value is assumed according to Jaki's formula. In all cases object of the present report, the default value was not changed.

Irrecoverable strains are concentrated at the interface between materials, by making use of interface elements (Section 4.1). Linear elastic mechanical behaviour has assumed for all interfaces with Mohr-Coulomb failure envelope.

4.2.3 Poroelastic model

In order to capture mechanical behaviour of saturated buffer, a poroelastic model has been implemented as user-defined constitutive routine in PLAXIS software. Considering that the software is not optimized for working with user defined models and large model, computational time increased tremendously when applying the poroelastic law to buffer material, thus imposing its use in a limited number of analyses. Stress-dependent elastic stiffness modulus E is defined as:

$$E = 3(1 - 2v')\frac{(1 + e_0)p'}{\kappa}$$

where p' is the current effective mean stress, κ swelling index and e_0 the initial void ratio. Being the material defined as perfectly non-linear elastic, no failure can occur therefore no strength parameters are needed. Although cases with linear elastic buffer are useful to compare the effects of different geometrical and mechanical parameters, analyses with non-linear elasticity are more realistic and their predictions should be considered the expected ones in reality.

4.3 Soil parameters used in the analyses

The identification of soil parameters has been carried out on the basis of available laboratory tests. Triaxial tests performed on 30/70 mixture for foundation bed material reported in Appendix 16 in Korkiala-Tanttu *et al.* (2007) were used to calibrate strength and stiffness parameters of foundation bed material. Calibration procedure is reported in Appendix 2. In order to compare the results with those obtained in previous calculations (Korkiala-Tanttu 2009), a linear elastic material was also used a preliminary calculation. However, due to shear and volumetric hardening mechanisms expected in the buffer-foundation interface region, only the results obtained with the Hardening Soil model are considered.

Bentonite pellets material parameters for Hardening Soil model were identified from data reported in Johannesson *et al.* (2010), and compared to previous analyses (Korkiala-Tanttu 2009) by replacing the Hardening Soil with linear elastic material.

Compressed bentonite blocks have been modelled as linear elastic, with stiffness parameter E' assumed as in Johannesson *et al.* (2010). The host rock and the canister are considered as a displacement boundary condition and therefore very stiff linear elastic material has been assumed. In addition, in two 3D analyses, poroelasticity was assumed for saturated buffer material, in analogy with Börgesson & Hernelind (2009).

Plastic deformations can occur at the interface between discrete elements of the model (blocks, foundation bed and bentonite pellets regions, rock, canister and buffer), therefore special interface elements described in Section 4.1 have been used.

Soil parameters specified in Table 4 and Table 5 have been adopted for 2D and 3D finite element analyses. For the Hardening Soil model, p_{ref} was assumed as the default value of $p_{ref} = 100$ kPa.

Table 4. *Soil parameters used in the analyses.*

Material model	Type	γ	φ′	c′	ψ	TCO	ν_{ur}	E_{50}^{ref}/E'	E_{oed}^{ref}	E_{ur}^{ref}/κ	m	e_0
		[kN/m³]	[°]	[kPa]	[°]	[kPa]	[-]	[MPa]	[MPa]	[MPa]	[-]	
Found. Bed HS	Drained	19.0	24.0	60.0	0.0	0.0	0.20	9.0	9.0	27.0	0.60	
Found.Bed LE	Drained	19.0					0.12	20.0				
Bent. pellets HS	Drained	16.0	27.0	40.0	0.0	0.0	0.20	3.28	1.64	16.4	1.0	
Bent. pellets LE	Drained	16.0					0.12	20.0				
Blocks LE	Drained	16.0					0.17	264.0				
Rock LE	Non porous	27.0					0.15	10000.0				
Canister LE	Non porous	27.0					0.15	10000.0				
Buffer LE	Drained	21.0					0.28	300.0				
Buffer PE	Drained	21.0					0.40			0.21		1.5

Table 5. *Interface input parameters (Mohr-Coulomb model).*

Interfaces	φ′	c′	ψ	TCO	ν'	E'
	[°]	[kPa]	[°]	[kPa]	[-]	[MPa]
Block-Block	24.0	0.0	0.0	0.0	0.2	90.0
Buffer-Rock	8.69	0.0	0.0	0.0	0.2	100.0
Pellet-Rock	10.0	0.0	0.0	0.0	0.2	20.0
Pellet-Buffer	5.0	0.0	0.0	0.0	0.2	10.0
Foundation-Rock	10.0	0.0	0.0	0.0	0.2	20.0
Foundation-Blocks	5.0	0.0	0.0	0.0	0.2	10.0
Foundation-Buffer	5.0	0.0	0.0	0.0	0.2	10.0
Foundation-Pellet	27.0	10.0	0.0	0.0	0.2	10.0
Canister-Buffer	5.0	0.0	0.0	0.0	0.2	10.0

4.4   Initialization and construction phases

In all axisymmetric and full 3D analyses the construction phases have been set in analogous way, thus reproducing the real construction sequence of the structure.

- Initial phase. Initial horizontal stresses are set by simulating the unsupported excavation of deposition tunnel and hole in the rock mass. Initial isotropic $K_0=1$ is set and equilibrium is reached after a so-called *Gravity loading* analysis.

- Installation of canister and saturated buffer blocks. The saturated buffer blocks (modelled as a continuum) are prestressed with a uniform mean stress of 7 MPa or alternatively 15 MPa (Figure 11). Interfaces along canister and buffer faces are activated.

- Installation of foundation bed, backfill blocks and pellets. Prestress load is still applied to buffer material.

- Expansion. Distributed loads applied to buffer cluster are deactivated, buffer material expands into backfill. Displacements are reset to zero before expansion.
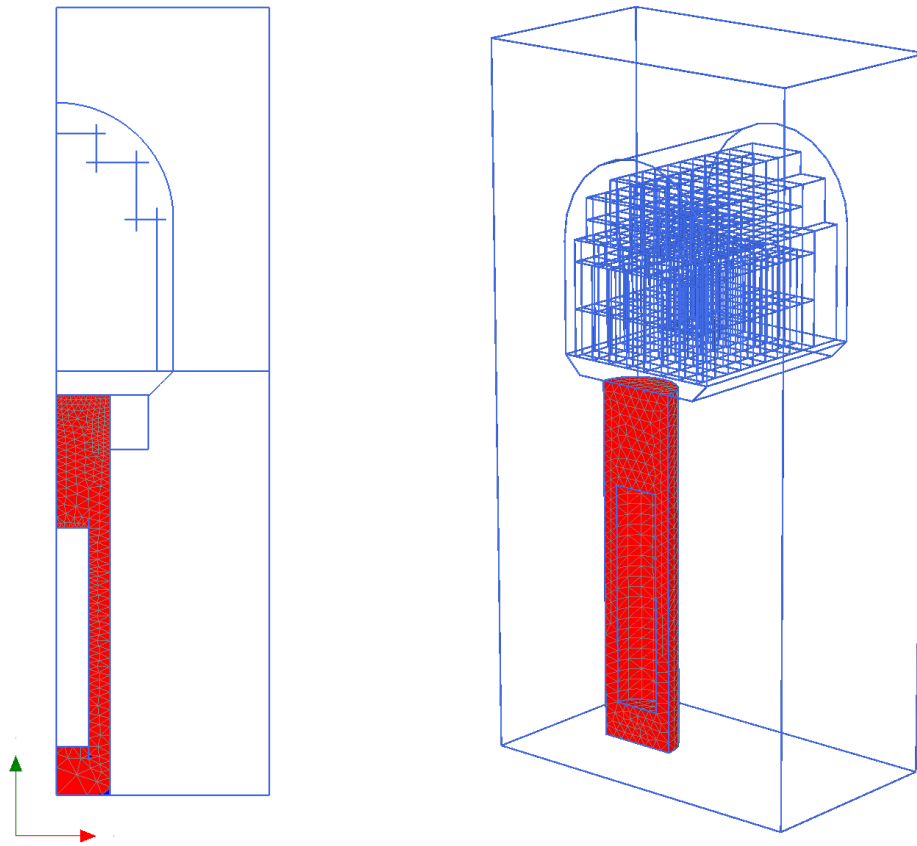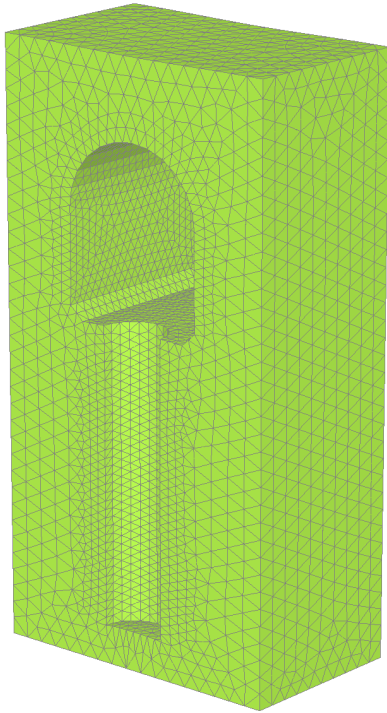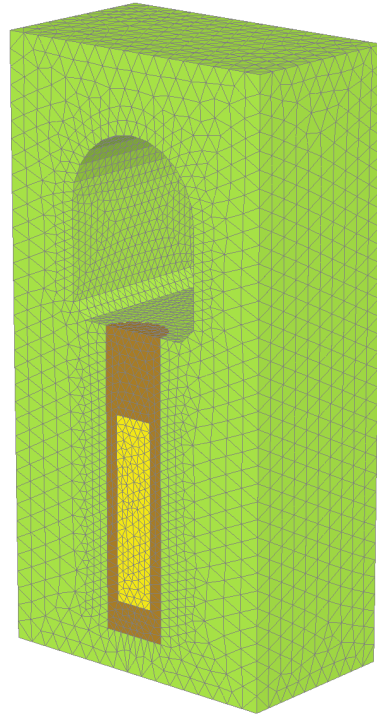

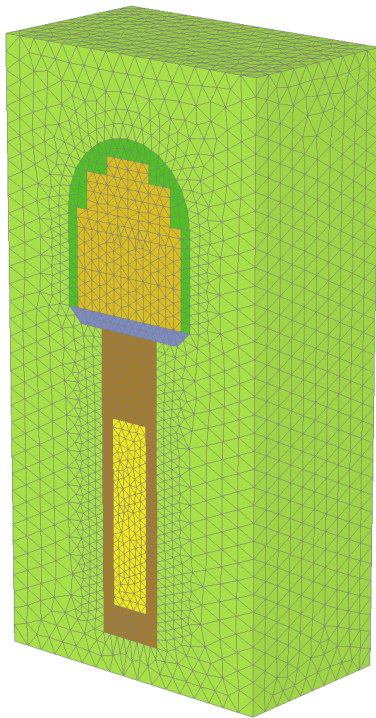***Figure 11.*** *Prestressed region in red (p' = 7 MPa, 15 MPa) for axisymmetric (left) and full 3D (right).*
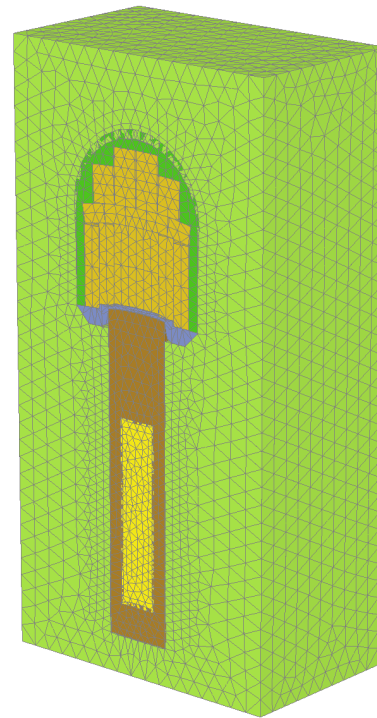
Figure 12. *a) Initial phase b) Installation of canister and buffer with isotropic prestress of 7-15MPa c) Installation of foundation bed, backfill blocks and pellets d) Removal of prestress, free expansion of buffer material into backfill foundation.*

5 MODELLING RESULTS

Case AX01
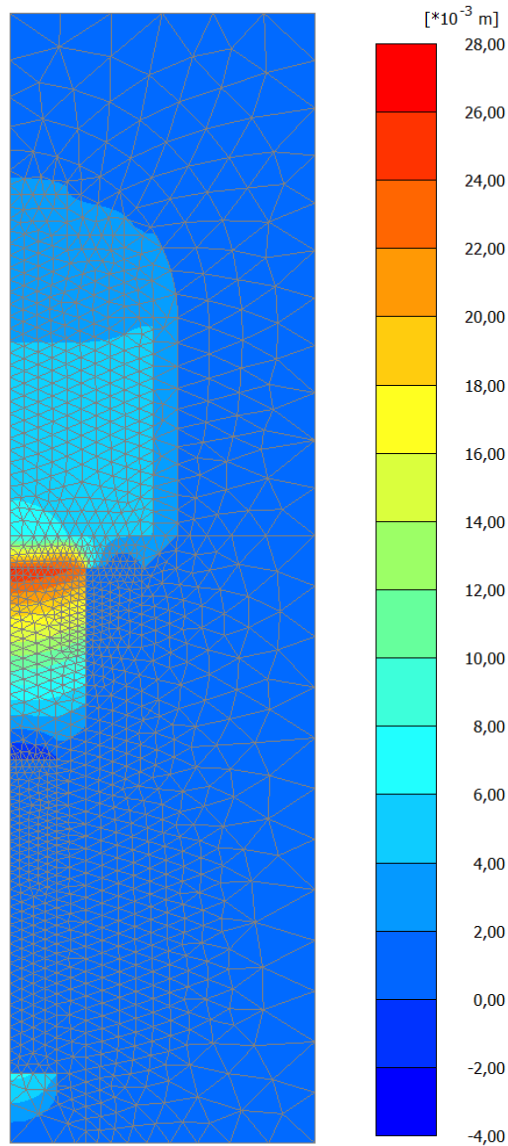
Figure 13. Vertical displacements.

In this axisymmetric analysis including the whole canister section and surrounding buffer in deposition hole, Hardening Soil model was used for foundation bed and a prestress of 7 MPa was considered. Most deformations are concentrated in the top 2.20 m above the canister top. Maximum vertical displacement after buffer swelling is about 26 mm, observed between buffer top and foundation bed. Considering the calibration purpose of axisymmetric analyses, further cases AX02 to AX09 have been carried out with reduced model size and are reported in Appendix 1.

3D01
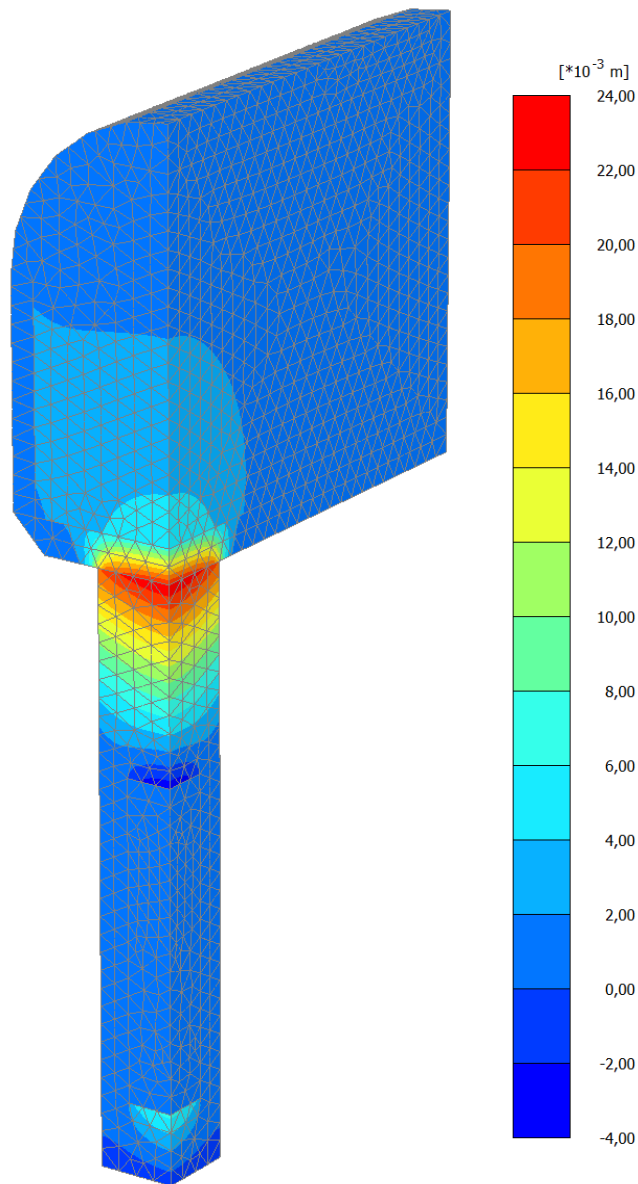
Figure 14. *Vertical displacements. Host rock excluded from visualization.*

The first full 3D analysis has been performed assuming linear elastic mechanical behaviour for all materials and 7 MPa swelling pressure. Analogously to 2D cases, elastic-perfectly plastic interfaces have been set at each contact between different materials. Due to symmetry of the problem, only a portion of one quarter of the model was taken into account. This was possible because the backfill blocks region was modelled as a continuum. The maximum vertical displacement resulting from calculations is 27 mm, observed at the backfill-foundation floor contact (Figure 14). Due to the assumption of linear elasticity in every part of the model (exception made for interfaces), this value should be regarded as an estimation of the order of magnitude although it should be not considered the expected one in reality.

Case 3D02
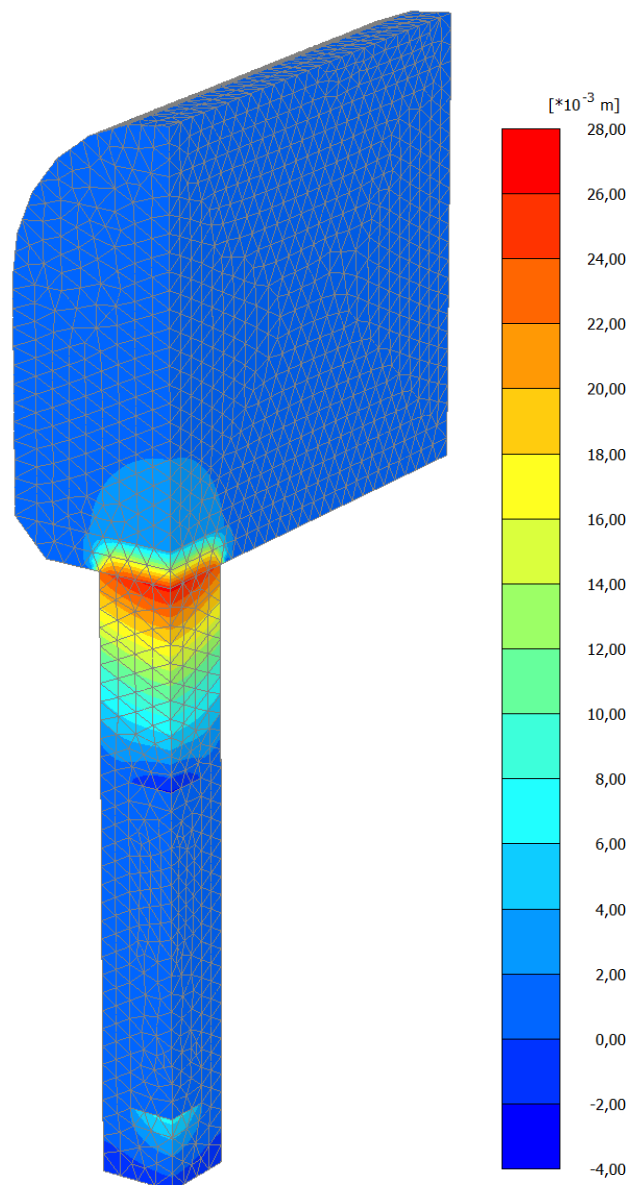
Figure 15. *Vertical displacements. Host rock excluded from visualization.*

In Case 3D02 Hardening Soil model has been used for foundation bed, and the maximum vertical displacement has been 26.6 mm in correspondence of a swelling pressure of 7 MPa (Figure 15).
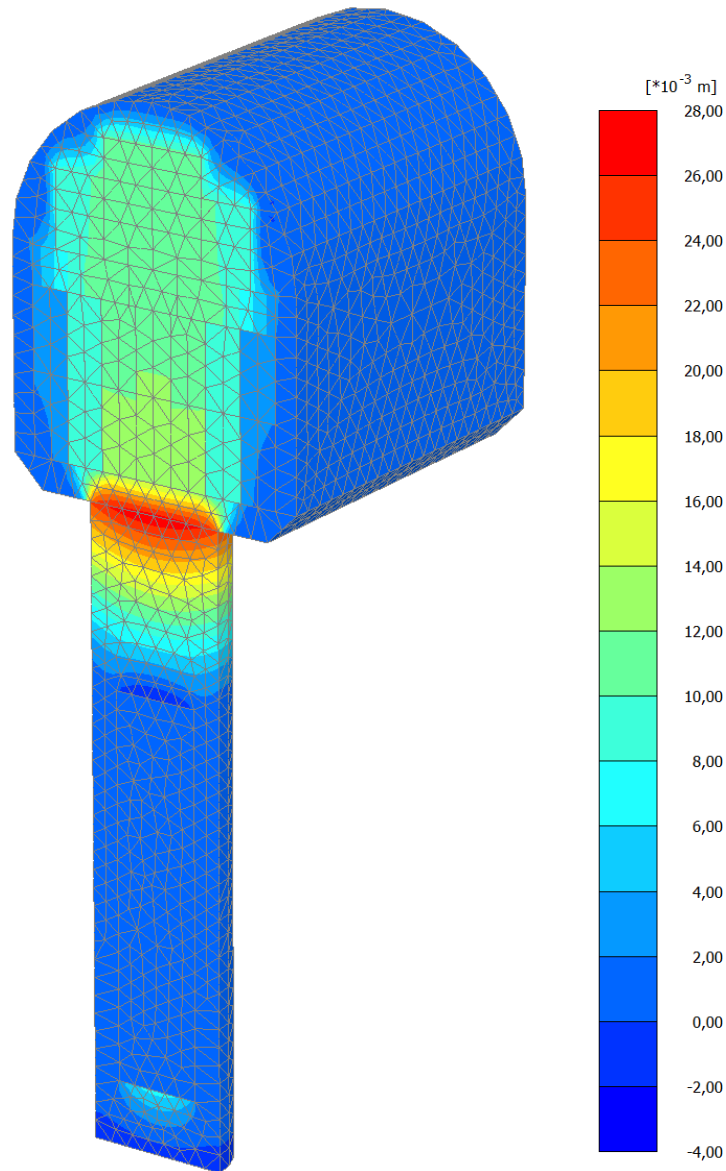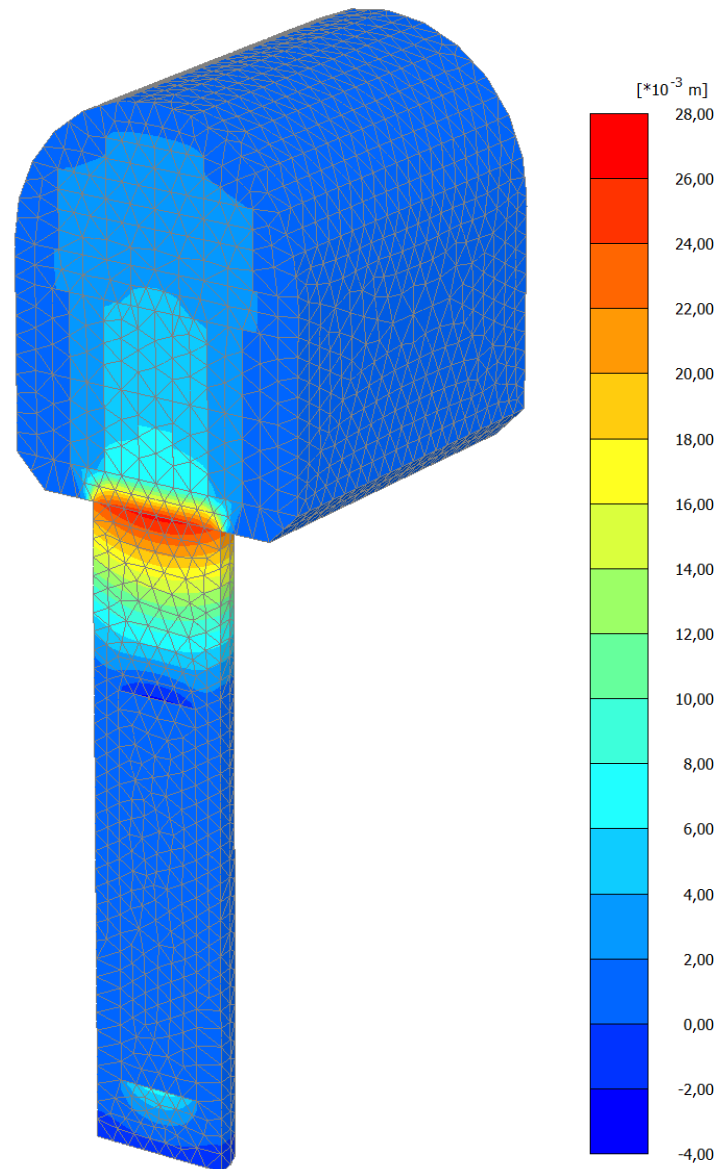
Case 3D03

Figure 16. *Vertical displacements. Host rock excluded from visualization.*

In case 3D03 Hardening Soil model has been applied to foundation floor and pellets material. Furthermore, all the blocks have been included in the geometry of the model, with elastic-perfectly plastic interfaces. Due to the block assembly, one of the two symmetry planes is lost, therefore the complexity of the model increased due to the larger number of finite elements needed. However, the finite element mesh was generated keeping the same element density as in previous cases. The maximum vertical displacement in case 3D03 is 27.8 mm (Figure 16) with 7 MPa prestress.

Case 3D04

Figure 17. *Vertical displacements. Host rock excluded from visualization.*

In case 3D04 Hardening Soil model has been applied to foundation floor. As in case 3D03 all the blocks have been included in the geometry of the model, with elastic-perfectly plastic interfaces. The maximum vertical displacement in case 3D04 is 26.8 mm (Figure 17).

Gauss points where irrecoverable plastic strains are generated are shown in Figure 18. It is evident that plasticized region is confined to a volume close to the deposition hole, where both shear and tensile failure are reached in block-block interfaces (i.e. sliding occurs), whereas mostly shear failure points are observed at the interface between buffer and host rock. In foundation bed on top of which backfill blocks are assembled, both shear and volumetric hardening occur. The former takes place close to expansion area, the latter further away moving towards the model boundaries. It is understandable that

far away from the expanded zone, the foundation soil is being compressed horizontally being allowed to expand very little due to the confinement exerted by host rock and the system of blocks above. The overall effect is a mainly volumetric strain whereas shear strains are concentrated in the area nearby the deposition hole where the blocks are displacing along the joints thus not being able to confine the material under swelling pressure.
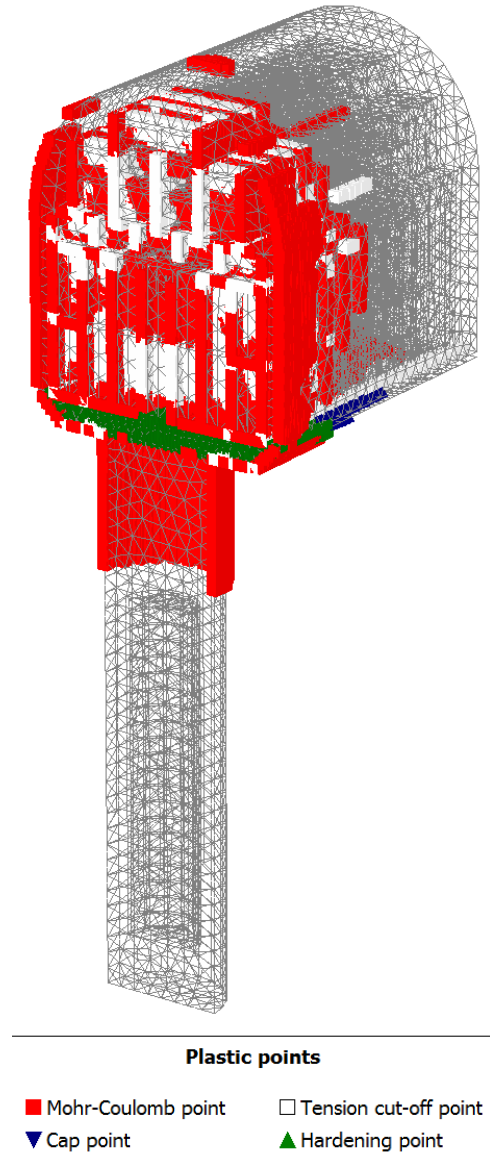

Plastic points

■ Mohr-Coulomb point   □ Tension cut-off point
▼ Cap point   ▲ Hardening point

Figure 18. Plastic points after expansion.

Deformed mesh of block assembly is shown in Figure 19. Clearly, deformations are compatible with buffer expansion mechanism, confirming the effectiveness of numerical model. In Figure 20 and Figure 21 vertical displacements are shown on a vertical section at the model longitudinal symmetry plane and on horizontal section at the bottom face of backfill blocks, respectively. All results confirm that the heave is concentrated in a region close to the projection of deposition hole. Figure 22 shows the

distribution of vertical displacements in buffer material at its top surface. The maximum value of 26.8 mm is observed at the centreline, slightly decreasing towards the external edges to a heave of 23 mm. The average heave is approximately 25 mm.
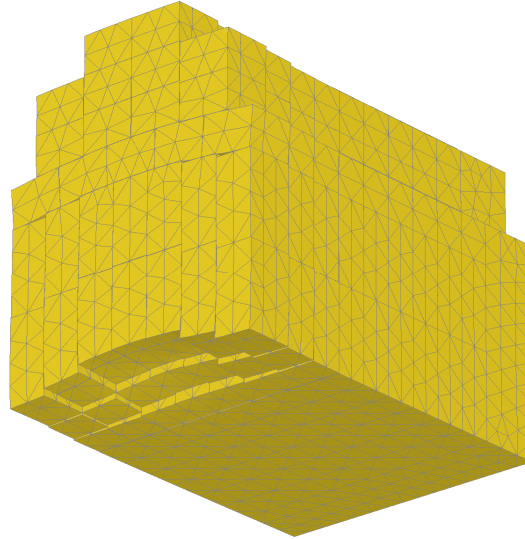

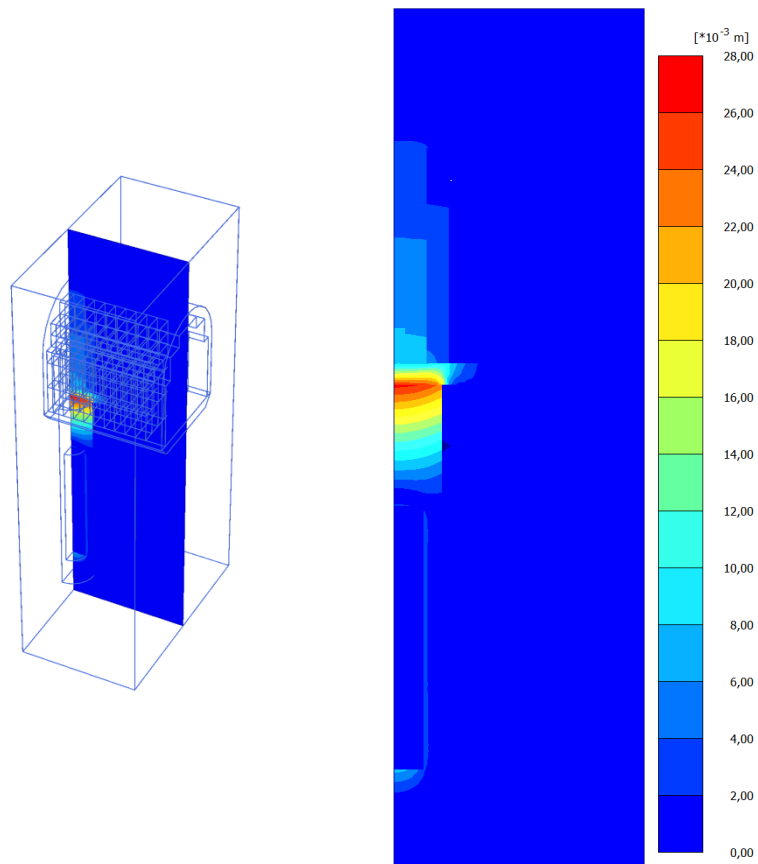*Figure 19. Deformed mesh of backfill blocks (magnification factor 50x).*

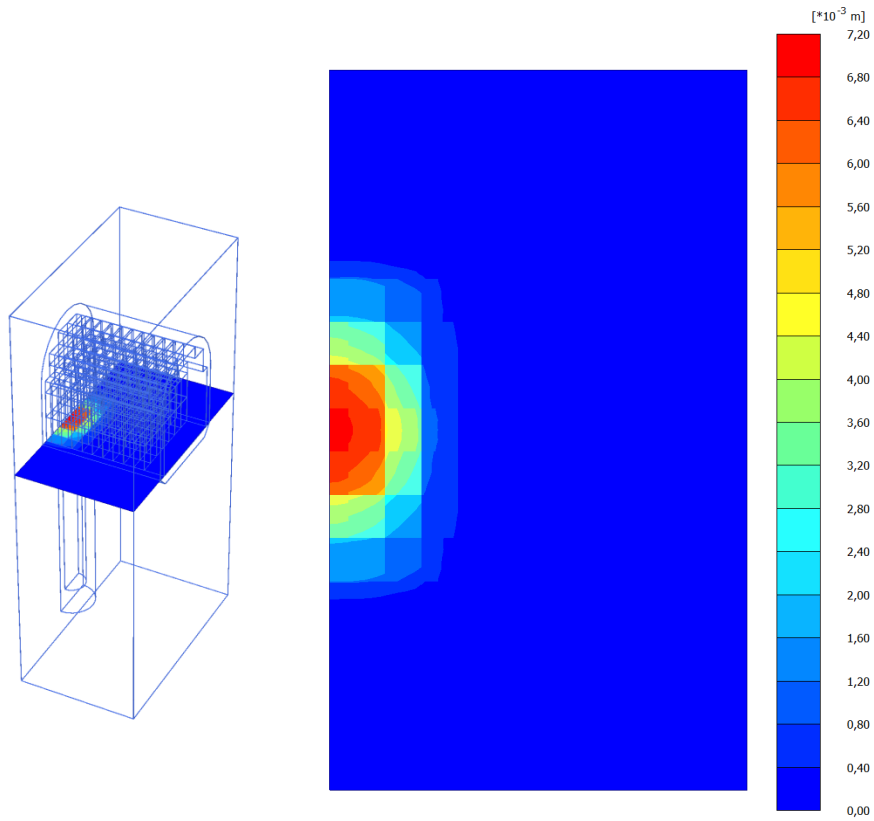*Figure 20. Vertical cross section at mid plane of blocks assembly. Vertical displacements.*

Figure 21. *Horizontal cross section at bottom surface of block assembly. Vertical displacements.*
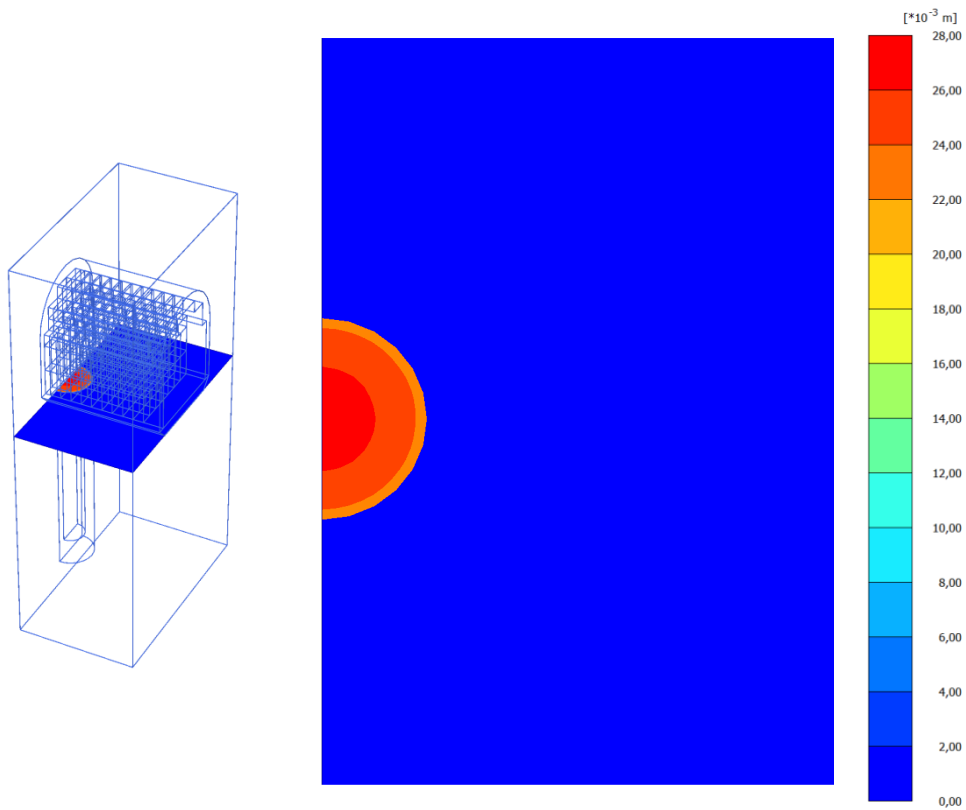

Figure 22. *Horizontal cross section at top surface of buffer. Vertical displacements.*
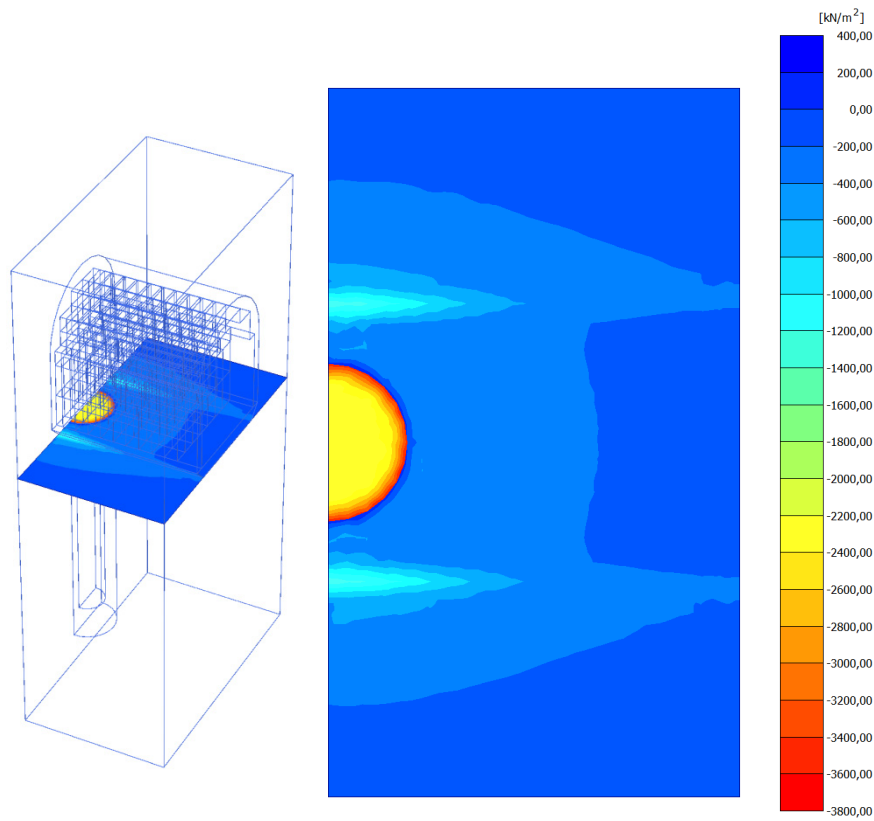
Figure 23. Mean stress at buffer top level (compression negative).

Contact pressure (mean stress) after expansion at buffer top surface is shown in Figure 23. The observed value varies from 2.4 MPa (centreline) to 3.8 MPa at lateral surface. Figure 24 shows the distribution of normal stresses at the buffer-foundation interface.
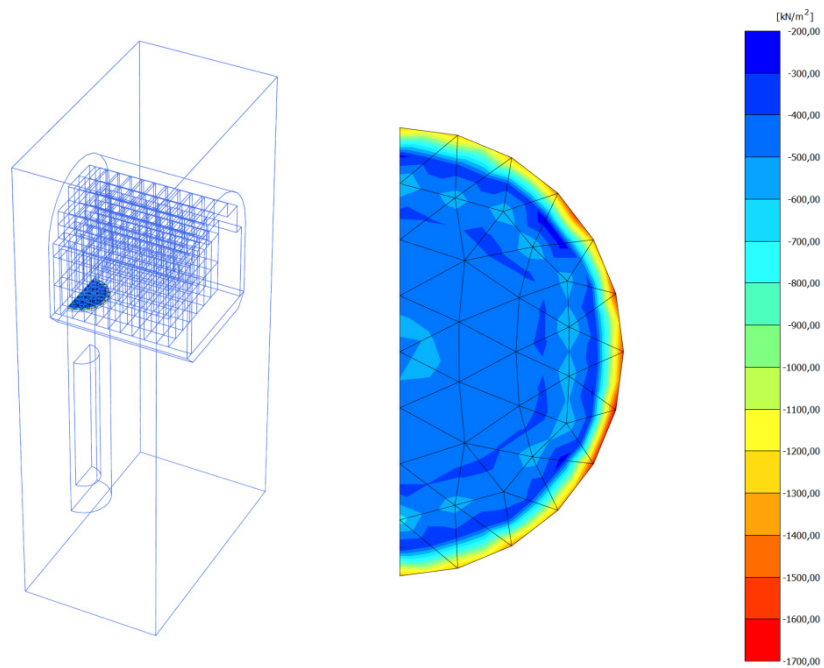

Figure 24. Contact pressure (normal stress) at buffer-foundation interface.
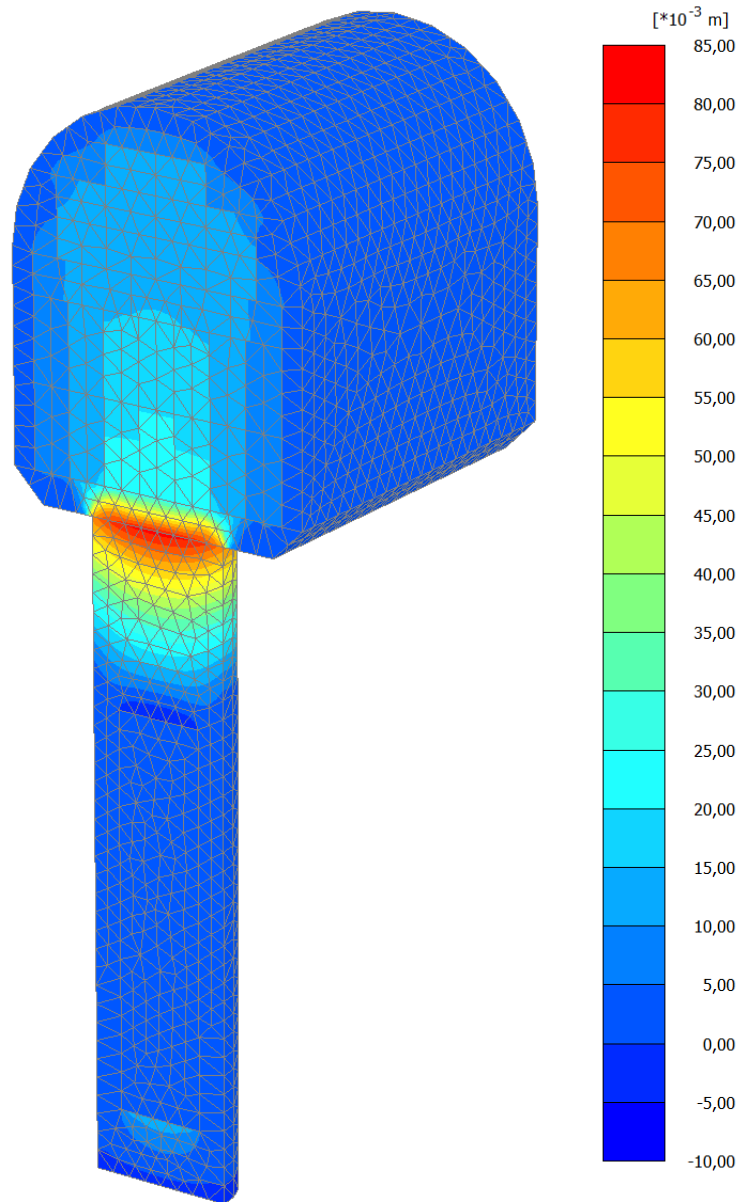
Case 3D04_II

Figure 25. Vertical displacements. Host rock excluded from visualization.

The use of logarithmic stiffness as assumed in poroelastic model used for buffer material in case 3D04_II generates a higher level of deformation than previous case 3D04. Maximum vertical displacement is 82 mm, observed at the interface between buffer and foundation bed (Figure 25). In terms of loss of density due to expansion of saturated buffer, Figure 26 shows the distribution of density in buffer material after swelling, calculated via the equivalence:

$$\varepsilon_v = (\rho_{initial} - \rho_{final}) / (\rho_{final} - \rho_{water})$$

from which stems:

$$\rho_{final} = (\rho_{initial} + \rho_{water} \, \varepsilon_v) / (1 + \varepsilon_v)$$

The requirement of minimum density of 1990 kg/m^3 is fulfilled everywhere in buffer material except a limited region close to the top surface.
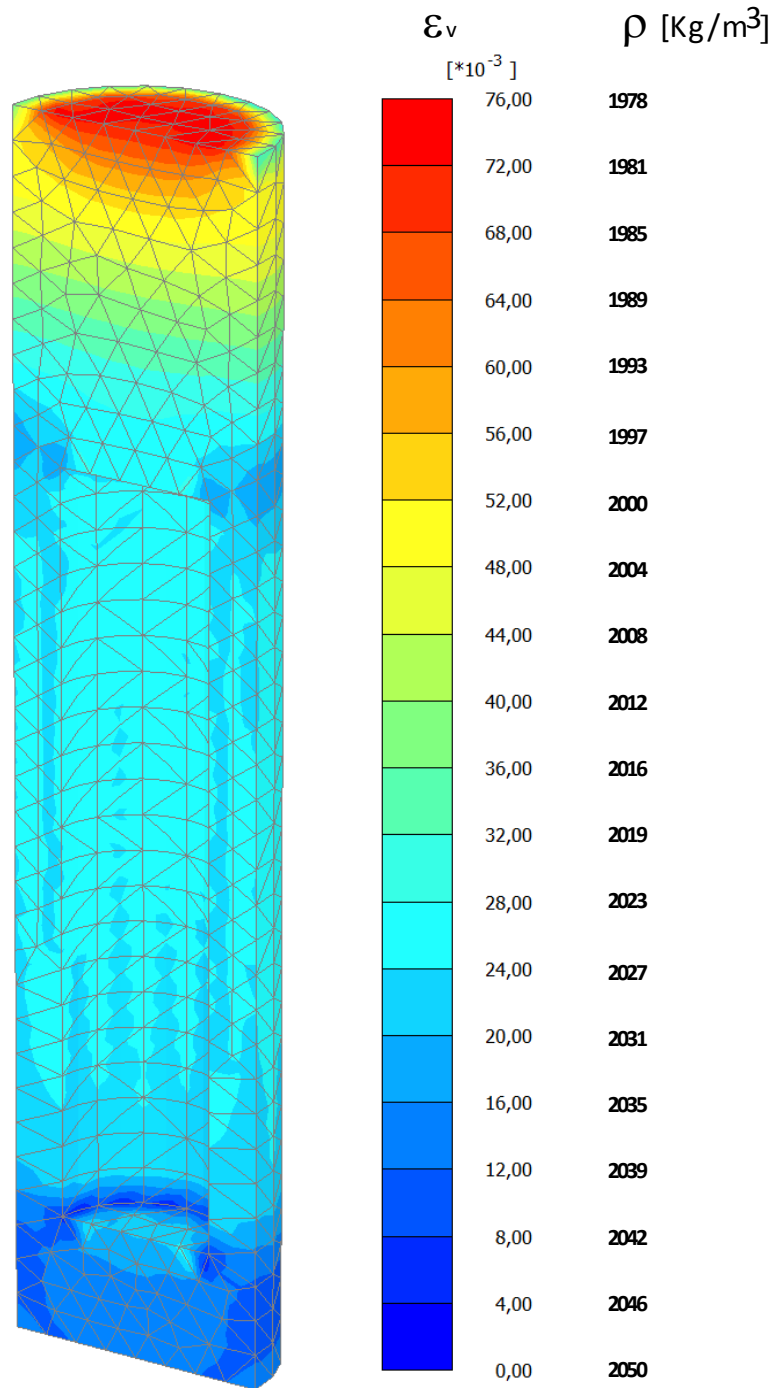

Figure 26. *Buffer material: volumetric strain, density after expansion.*
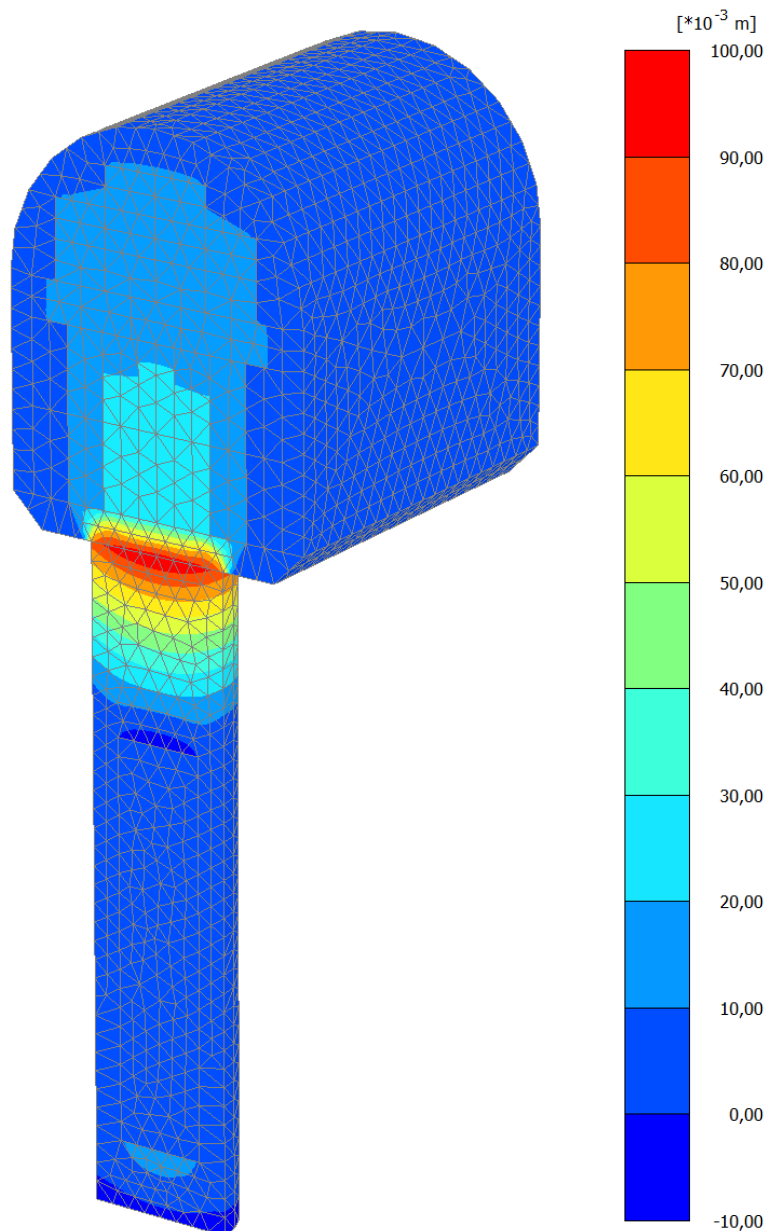
Case 3D04_III

Figure 27. *Vertical displacements. Host rock excluded from visualization.*

In the third variation considered for standard case 3D04, still a poroelastic material model is used for buffer blocks and an initial mean stress distribution of 15 MPa has been applied as precompression stress. Consequently, the resulting vertical heave increases to 99 mm (Figure 27). As in previous case, saturated density after swelling is plotted with volumetric strain (Figure 28): the region where the minimum density condition is violated is getting wider, but still reasonably confined in the vicinity of topmost surface.
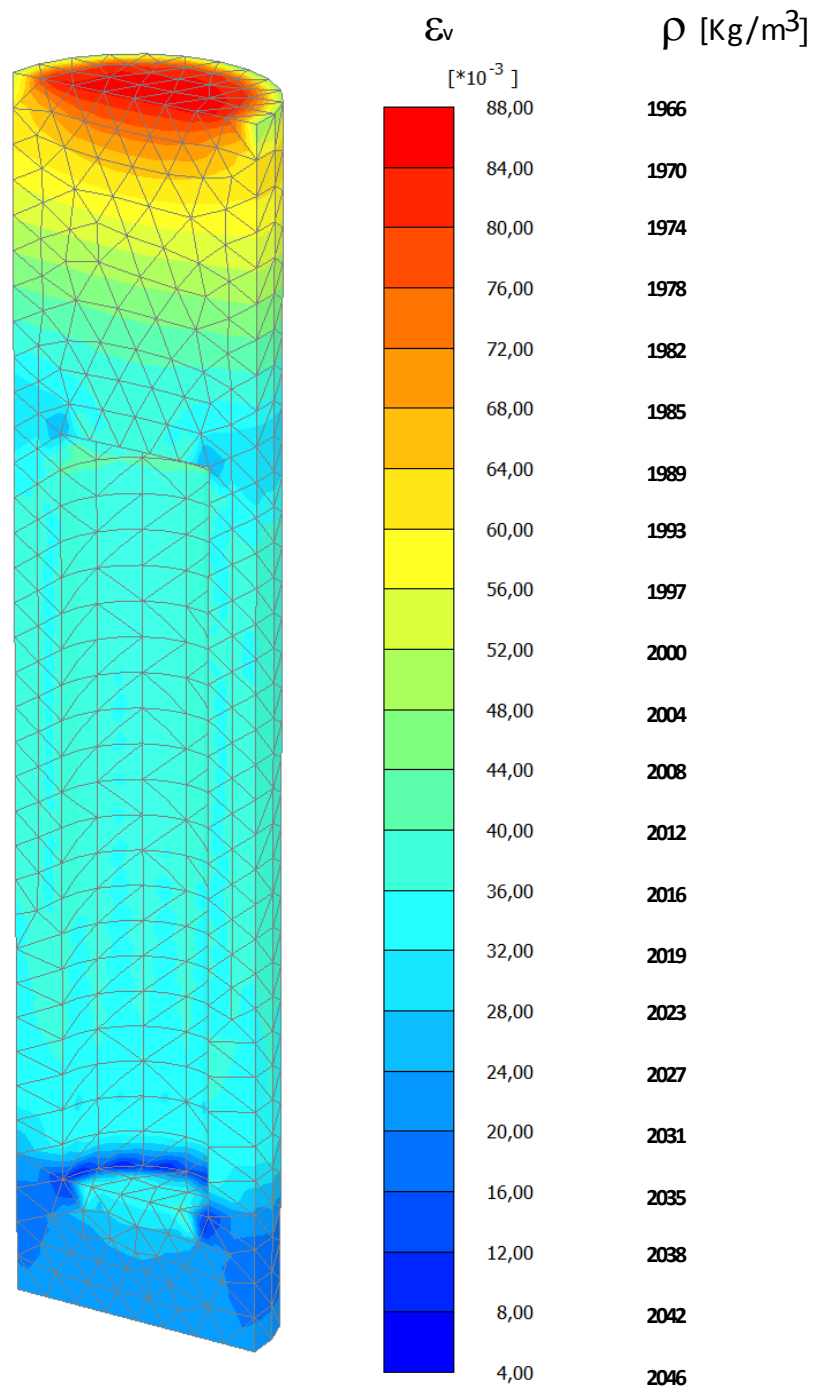
Figure 28. *Buffer material: volumetric strain, density after expansion.*
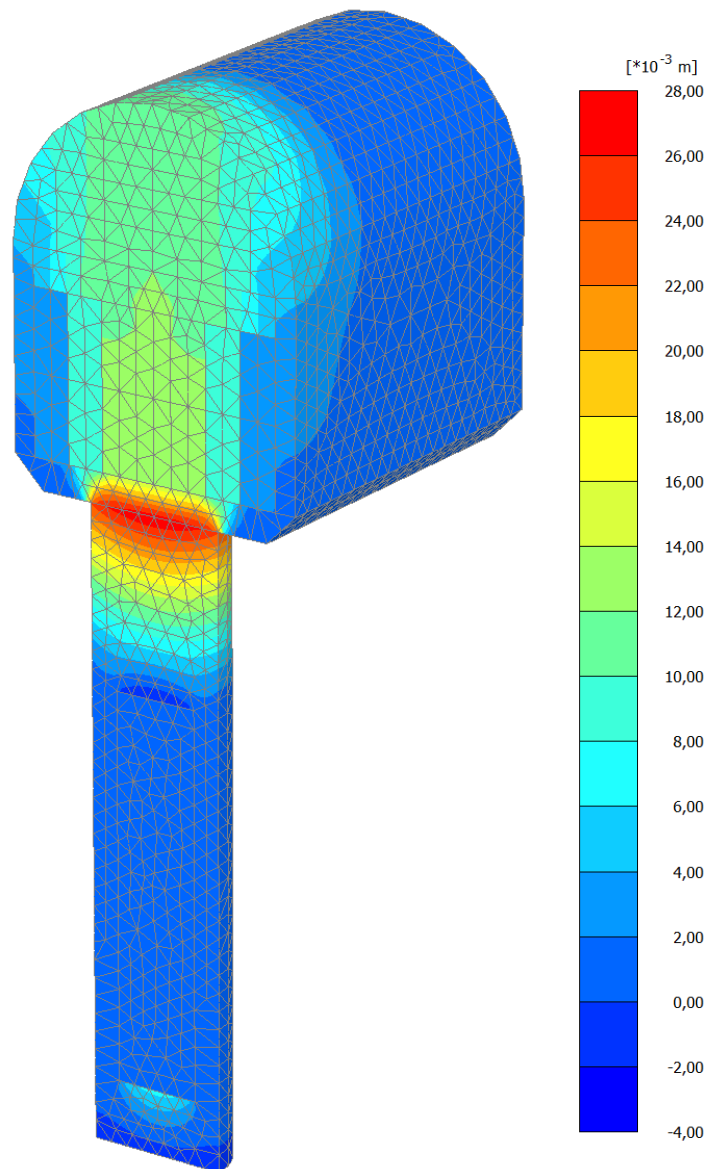
Case 3D05

Figure 29. *Vertical displacements. Host rock excluded from visualization.*

A gap between pellets and host rock is simulated by reducing to zero the elastic stiffness of the corresponding interface behaviour. The effect is limited to the vertical displacement of upper part of backfill system, with a slight increase of vertical heave at buffer level (27.8 mm versus 26.8 mm of case 3D04). The increased effect on topmost part of the model is evident from comparison of Figure 29 and Figure 17.

Case 3D06

In case 3D06 the intersection between buffer and foundation bed of the backfill system has been modified assuming that in the execution phase there will be the need of a local enlargement to ease the insertion of canister. The case considered here is that the shape of such enlargement is such as shown in Figure 30. Assuming the left side of the model as symmetry plane implies that the wedge is also present on the opposite side, which is not the case. Anyway, in this case the assumption is conservative, as a double over-excavation increases the predicted vertical displacement.
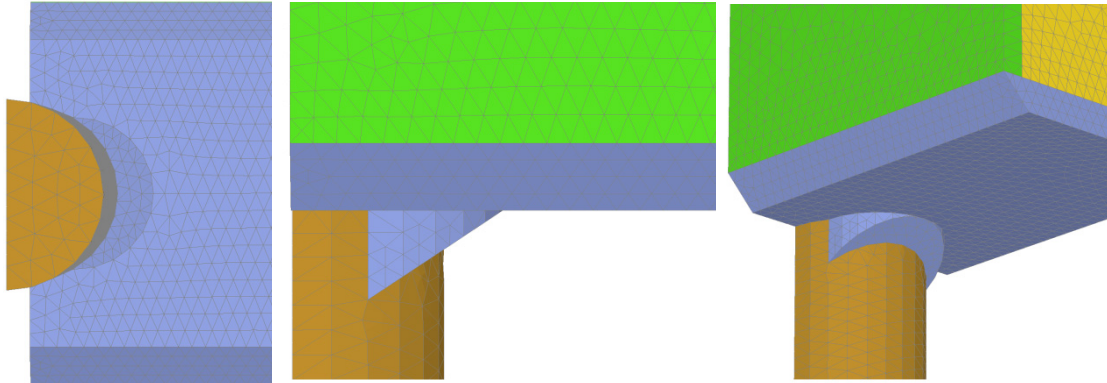

Figure 30. Shape of intersection between buffer and foundation floor (left: bottom view, centre: side view, right: perspective view).

In this case it is assumed that the enlargement is filled with the same material such as used in foundation bed (30/70 mixture).

A maximum vertical displacement of 28 mm is observed at deposition hole's centreline (Figure 31).
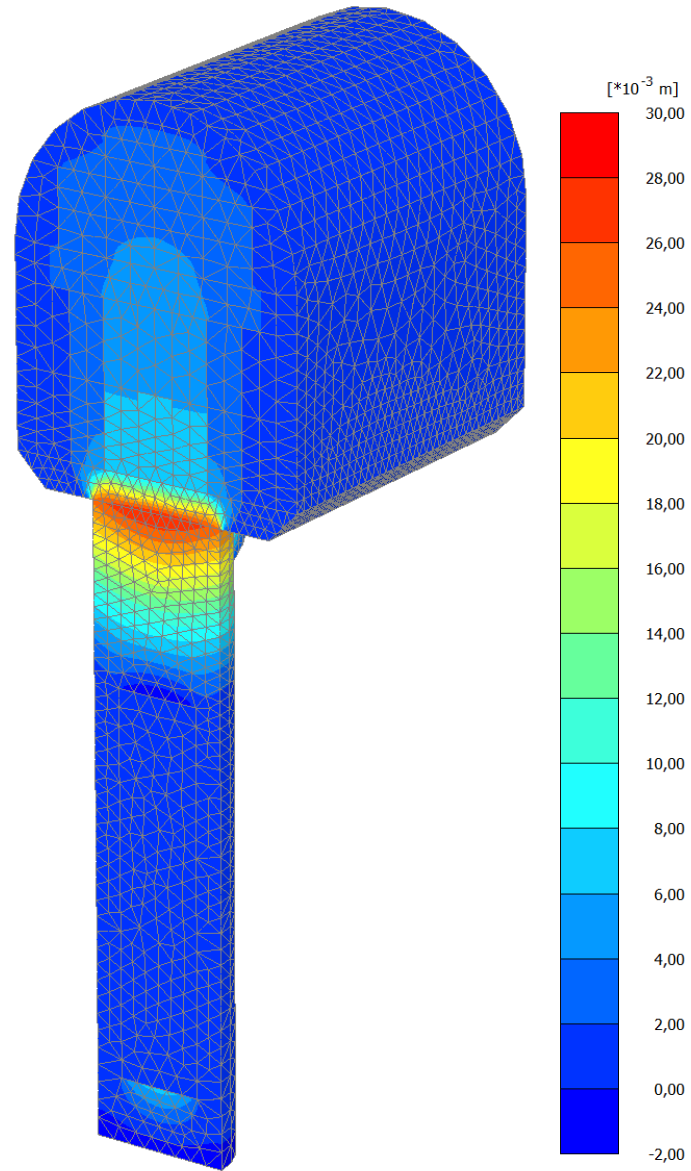
Figure 31. *Vertical displacements. Host rock excluded from visualization.*

Case 3D07
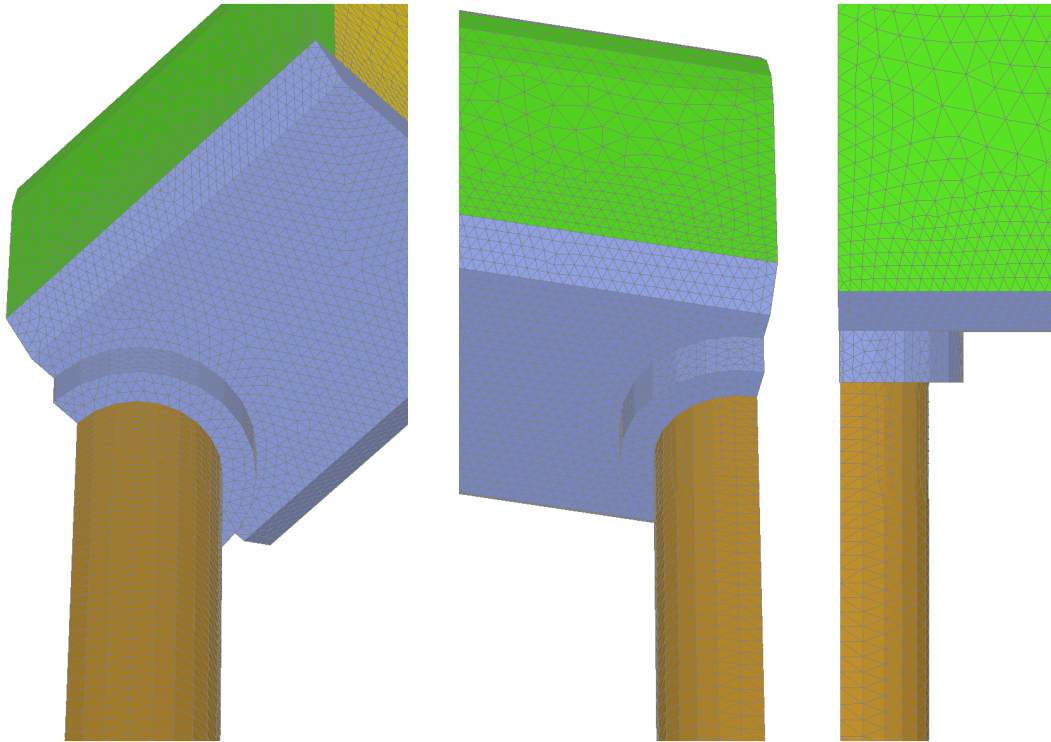
Figure 32. *Shape of intersection between buffer and foundation floor (left, centre: perspective view, right: side view).*

Similarly to case 3D06, an enlargement of upper part of buffer/foundation bed intersection has been considered. In this case the shape of the over-excavation is a full-section ring around the buffer topmost part (Figure 32).

Maximum vertical displacement is 29.5 mm, with the distribution shown in Figure 33.

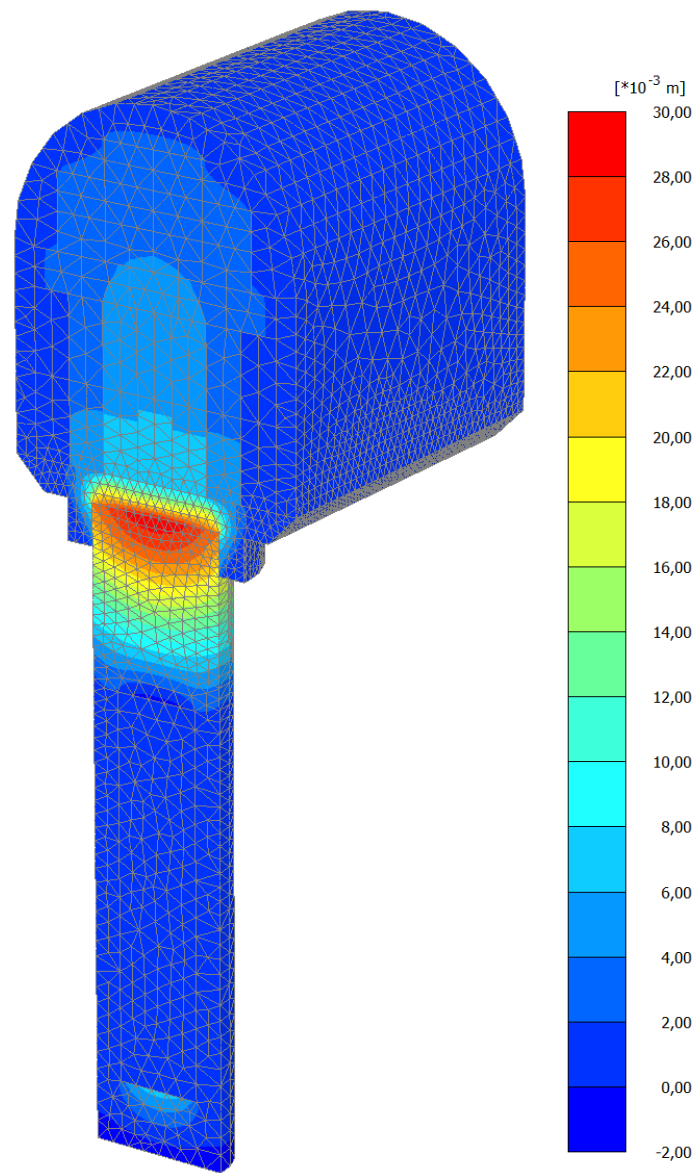**Figure 33.** *Vertical displacement. Host rock excluded from visualization.*

Case 3D08
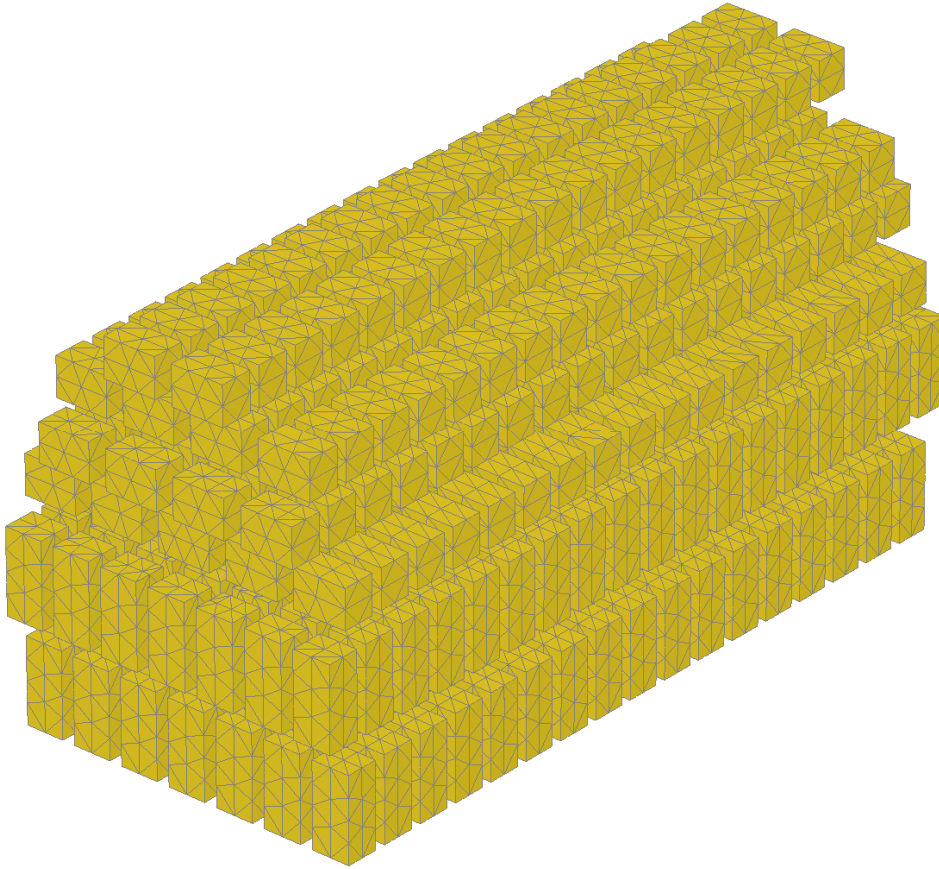
Figure 34. Overlapping blocks.

In this case it is considered a backfill block assembly with bentonite blocks overlapping between two contiguous horizontal block layers. The interlocking increases with respect to previous cases, and the penetration of buffer material into backfill is expected to be lesser. Since the full geometry of the model needed to be considered, the model resulted in 156 000 finite elements and 275 000 nodes, with an average element size of 85 mm.

The maximum vertical upward displacement is 26.6 mm. The distribution of vertical displacements in a cross section through the centreline of deposition hole is shown in Figure 35.

Figure 35. *Vertical displacements.*

Case 3D08_II

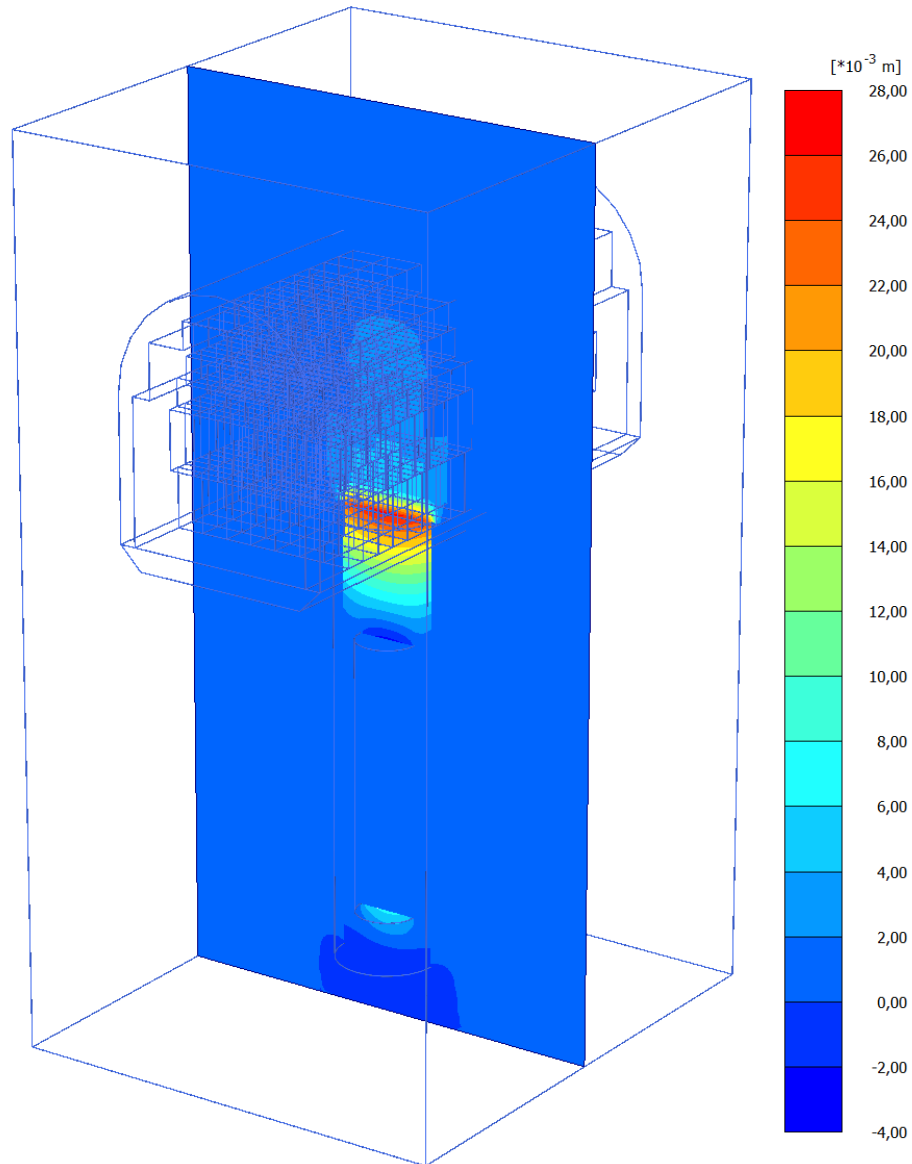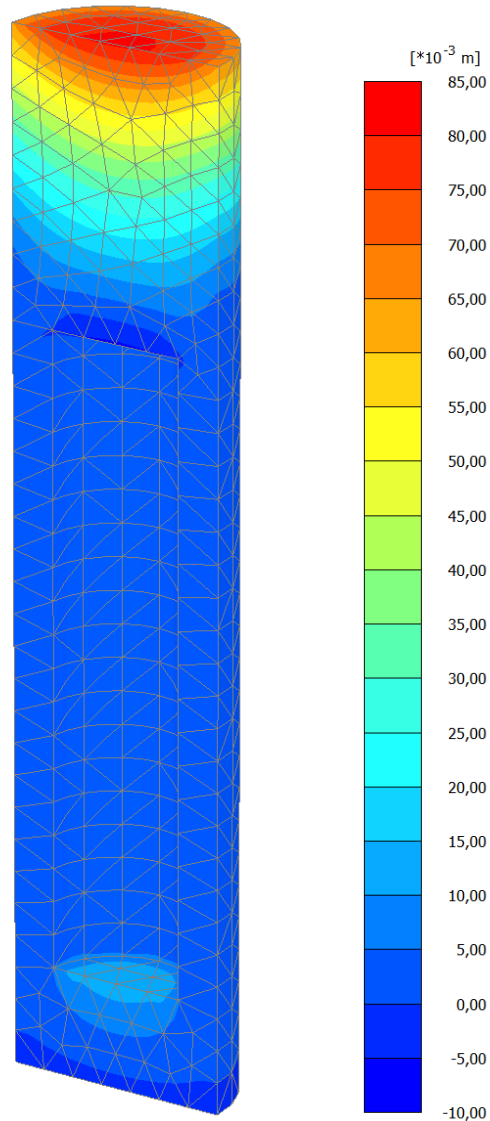***Figure 36.*** *Vertical displacements in buffer region (vertical cross section).*

Analogously to case 3D04_II, in present case 3D08_III linear elastic model for buffer material has been replaced by logarithmic stiffness (poroelasticity). The aim of this case is to check the effect of staggering the blocks in longitudinal direction instead of setting them in a perfectly overlapping configuration. Indeed, the maximum vertical displacement measured in a cross section along the deposition hole centreline is 81 mm, thus showing a very limited reduction of heave compared to case 3D04_II, where the heave results in 82 mm. For the sake of completeness, also volumetric strain and density after swelling are plotted in Figure 37, thus showing that the deformed buffer is in most part compatible with the required minimum density of 1990 kg/m^3.
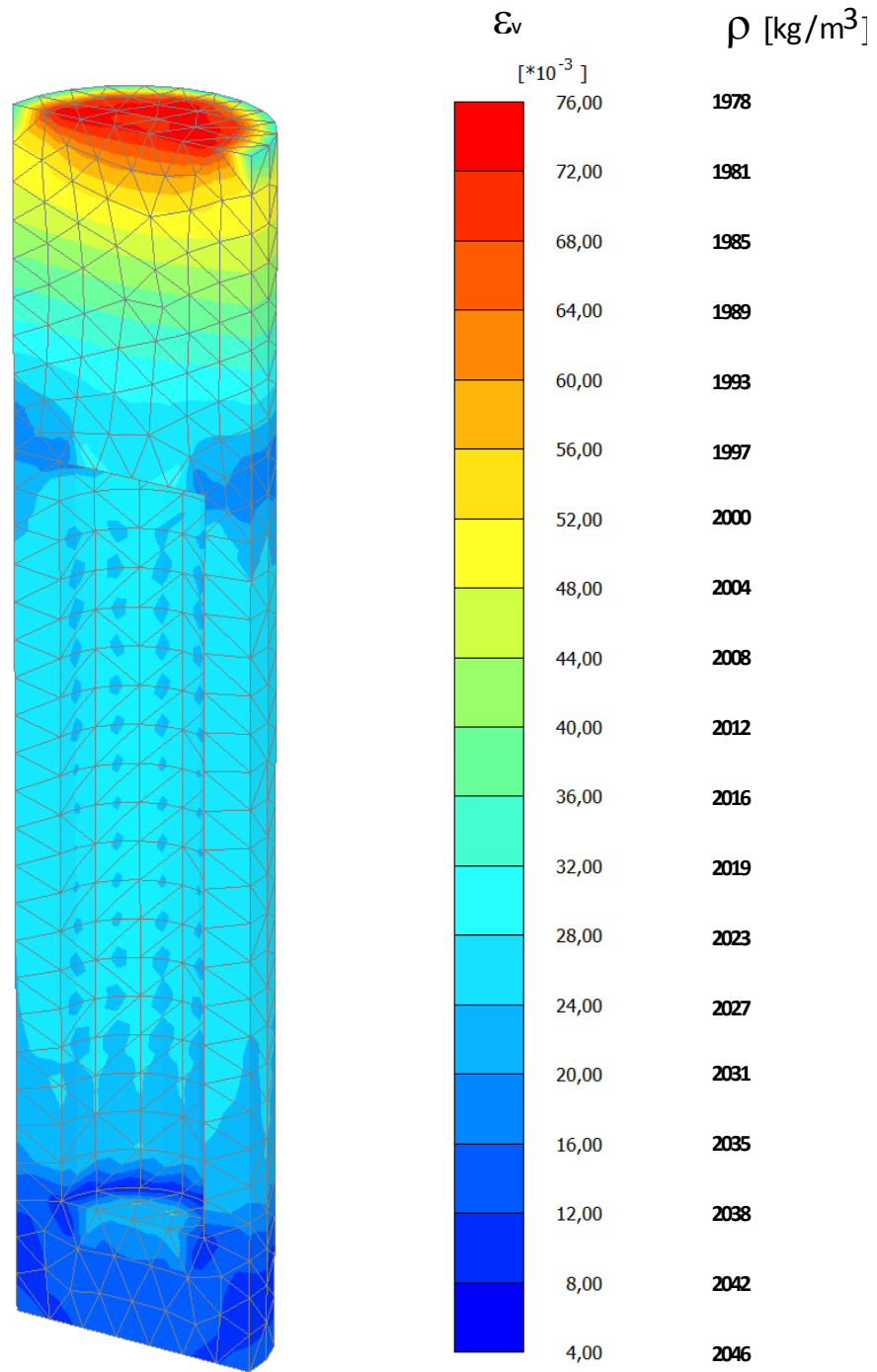
Figure 37. *Buffer material: volumetric strain, density after expansion.*

Case 3D08_III
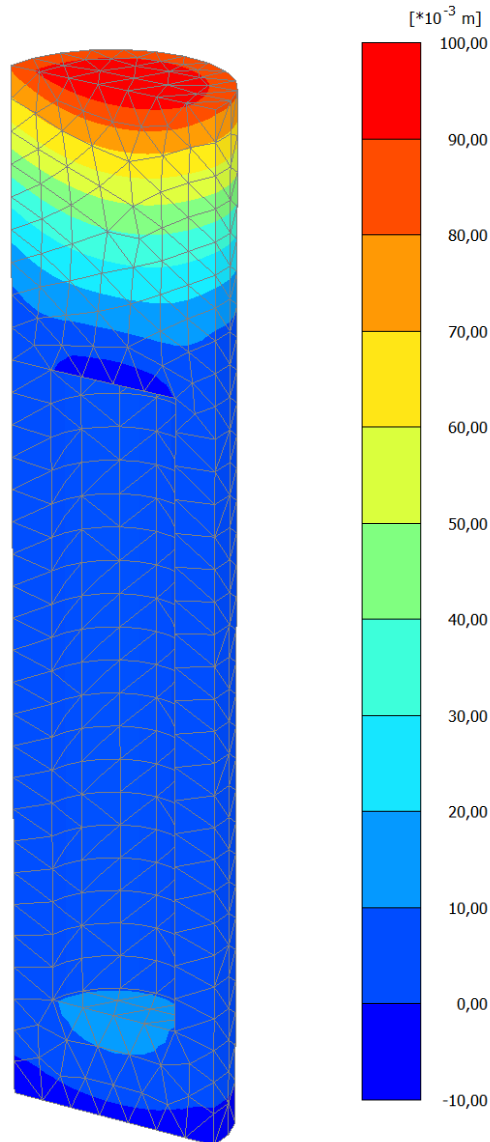
Figure 38. *Vertical displacements in buffer region (vertical cross section).*

On applying a swelling pressure of 15 MPa with the same material models as in previous case 3D08_II, a maximum vertical heave of 98 mm is obtained. The plot of volumetric strain and final density (Figure 39) shows as usual only a limited region of buffer where the density drops below 1990 kg/m^3.
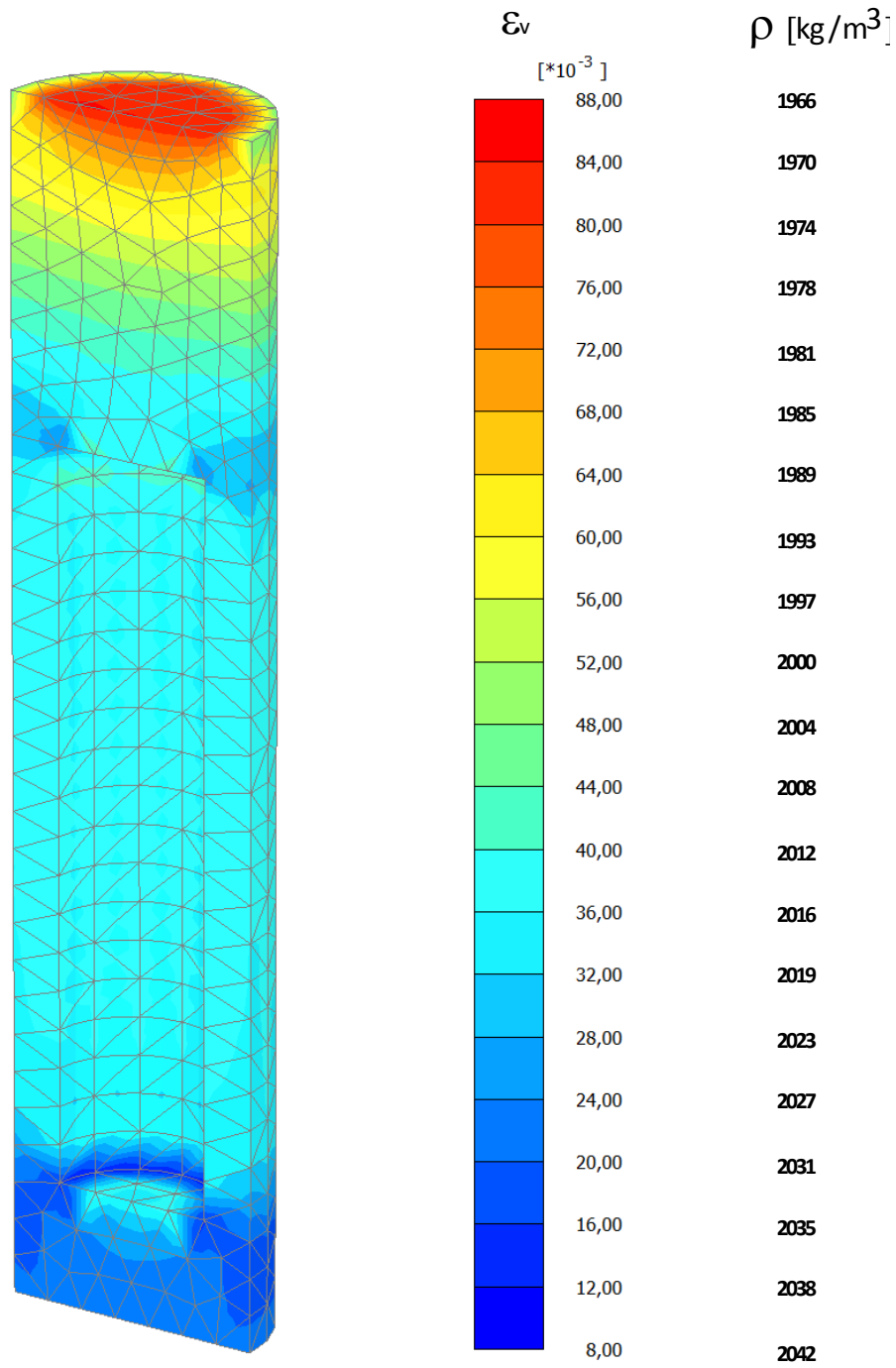
Figure 39. *Buffer material: volumetric strain, density after expansion.*

Case 3D09
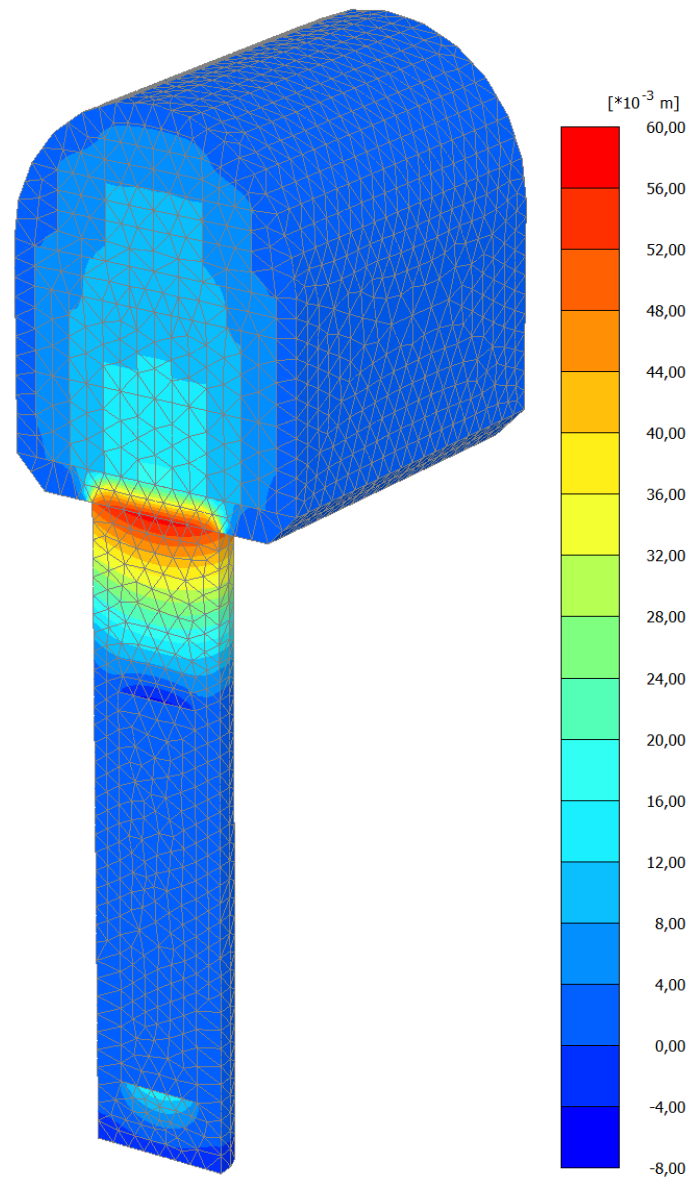
Figure 40. *Vertical displacement. Host rock excluded from visualization.*

Case 3D09 is concerned with a swelling pressure of 15 MPa, which is considered as the upper bound. The maximum vertical displacement is 58 mm, with the uniform distribution shown in Figure 39, and a contact pressure ranging from 5 MPa to 8 MPa at the interface between buffer and foundation bed (Figure 41). As for Gauss points where plastic deformations occur, Figure 43 shows their distribution in finite element model. Comparing it to the case where 7 MPa of swelling pressure are applied (Case 3D04, Figure 18), it appears that the distribution is quite similar, with only a slightly higher concentration in the upper part of backfill system. Hardening point distribution in foundation bed seems not to be significantly affected by the increased swelling pressure. Figure 42 shows the distribution of normal stresses at the buffer-foundation interface.

Figure 41. *Mean stress at buffer top level (compression negative).*

Figure 42. *Contact pressure (normal stress) at buffer-foundation interface.*

Plastic points

■ Mohr-Coulomb point   □ Tension cut-off point
▼ Cap point   ▲ Hardening point

Figure 43. *Plastic points after expansion.*

6 DISCUSSION OF THE RESULTS

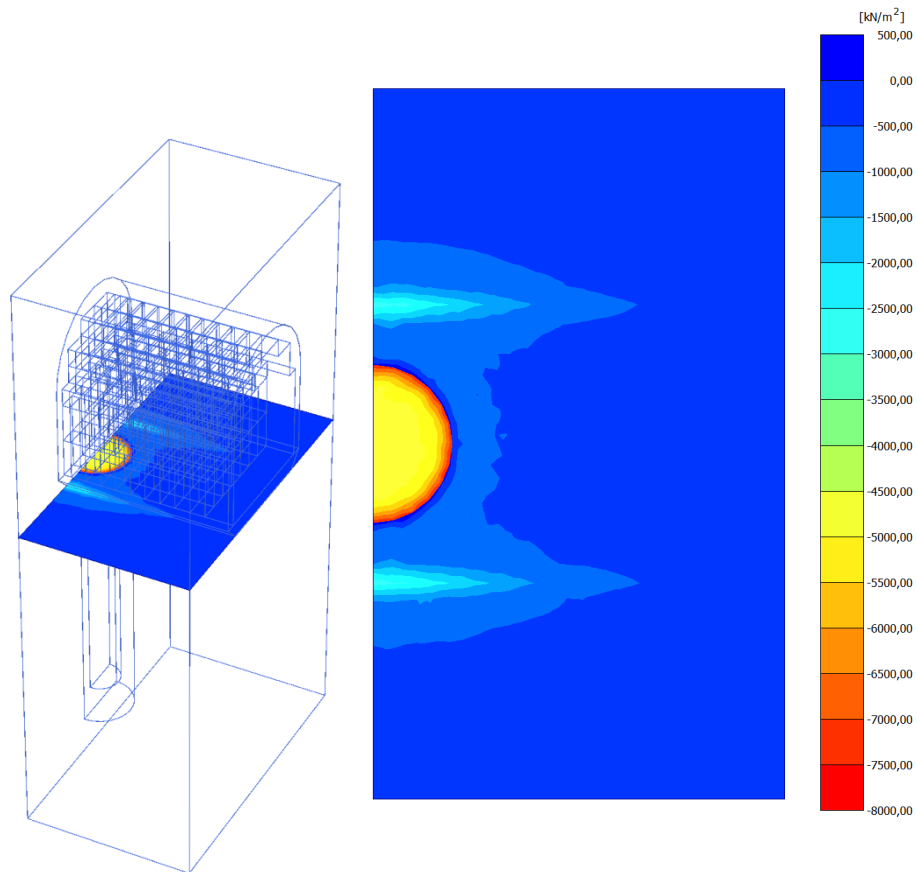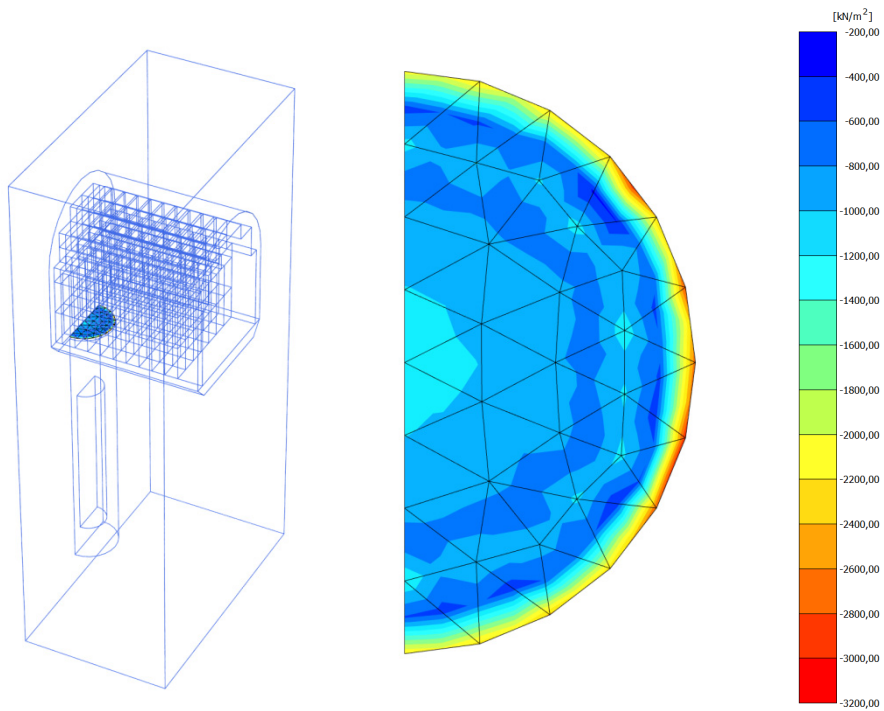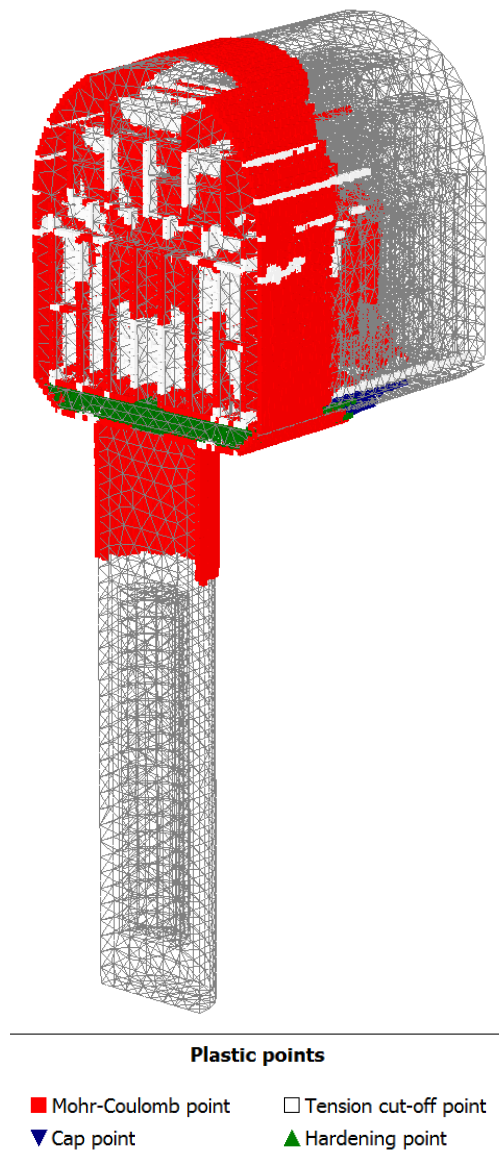The finite element analysis' results enable to gain insight on the deformation mechanism of the buffer-backfill system. From the picture of distribution of vertical heave through the section (e.g. Figure 29), appears that the pressure exerted at the bottom of foundation bed by the swelling buffer is transmitted to the top of the stack of backfill material with a lateral spreading through blocks mainly along their horizontal and vertical interfaces.

Finite element analyses performed confirmed that the heave of buffer material into backfill is limited to less than about 100 mm. In the following Table results are summarized by grouping the analysed cases in three series in order of relevance to the study. The results of the first series of 3D calculations (Series 1), with poroelastic material applied to buffer region, a second series of 3D models (Series 2) with linear elasticity for buffer material and a third series of axial symmetric simplified models (Series 3) analysed mainly with calibration purposes.

Table 6. Maximum vertical displacement.

Series 1		Series 2		Series 3	
Analysis type	**Max. Heave [mm]**	**Analysis type**	**Max. Heave [mm]**	**Analysis type**	**Max. Heave [mm]**
3D04_II	82.0	3D01	27.0	AX01	26.0
3D04_III	99.0	3D02	26.6	AX02	17.0
3D08_II	81.0	3D03	27.8	AX03	20.0
3D08_III	98.0	3D04	26.8	AX04	19.0
		3D05	27.8	AX05	20.3
		3D06	28.0	AX06	19.0
		3D07	29.5	AX07	21.0
		3D08	26.6	AX08	20.5
		3D09	58.0	AX09	19.8

As argued in Section 0, the limit saturated density ensuring a proper sealing of deposition hole was estimated in 1990 kg/m^3 (i.e. unit weight 19.50 kN/m^3). Starting from an initial saturated density value of 2050 kg/m^3, unit weight 20.11 kN/m^3 (Korkiala-Tanttu 2009), the maximum admissible heave can be calculated as:

$h0$ $(\gamma_{initial} - \gamma_{final}) / (\gamma_{final} - \gamma_{water}) = 2.20$ $(20.11\text{-}19.50)/(19.50 – 10.00) = 141$ mm

As shown in Table 6, also when a swelling pressure of 15 MPa is applied the vertical heave remains below the limit value with a good margin of safety. However, a criterion based on maximum heave only ensures that the maximum density is not exceeded in average within the swelling buffer above canister top. Locally, as shown in Figure 26, Figure 28, Figure 37 and Figure 39, the density drops below the threshold value of 1990 kg/m^3. Nevertheless, the region involved is always very limited and concentrated

towards the top of deposition hole, thus not compromising the effectiveness of the system.

In detail, analyses of Series 1, which are supposed to provide the most valuable results both qualitatively and quantitatively, give a vertical heave of 81 mm to 82 mm depending on the block assembly (3D08_II and 3D04_II, respectively) with a swelling pressure of 7 MPa, whereas the vertical heave reaches 98 mm and 99 mm with 15 MPa and same two different assemblies (3D08_III and 3D04_III, respectively).

Analyses of Series 2 have been performed with the simplifying assumption of linear elastic buffer material. Although it appears that the assumption is too crude as vertical displacements are strongly underestimated in absolute, the results obtained should be considered in mutual comparison to evaluate the effect of variations of geometry and other material parameters.

3D01 and 3D02 were performed under the assumption of continuum material for backfill blocks and should be considered preparatory analyses. Interfaces between blocks were introduced from case 3D03 onwards. 3D04 is the standard case for 3D analyses, with Hardening Soil model for foundation bed and linear elastic material for buffer region. In 3D05 a roof gap has been introduced, but the results were not significantly affected.

In order to simplify the deposition procedures, it is likely that a chamfer is needed at the intersection between deposition hole and deposition tunnel. In these analyses two different cases have been considered, one with wedge-shaped chamfer (3D06) and a second case with square-torus chamfer (3D07). It is assumed that the gap created by the chamfer is then filled with the same material used for foundation floor. The effect on vertical deformations is in that, due to lesser confinement in the upper part of buffer, the vertical upward displacement becomes larger. Still, from the quantitative point of view, the increased swelling appears negligible compared to the case without chamfer.

Case 3D08, where the arrangement of backfill block modules is such that there's half block overlapping between contiguous block layers, shows that the longitudinal interlocking does not implies a significant increase of the system rigidity, and therefore the higher effort required to ensure an overlapping of the blocks in longitudinal direction should be considered thoroughly.

Plastic points where Mohr-Coulomb failure criterion has been violated are concentrated in lateral interfaces in the upper part of buffer material, though the precompression mean stress was applied to the whole structure (Figure 12 right). This means that, because of the confinement exerted by host rock, the upward swelling occurs mainly in the part of buffer material between canister and foundation bed.

As for the information obtained by Series 3 of axial symmetric analyses, the influence of over-excavation appears very limited, as it results in a range of upheaval between 19 mm and 21 mm varying from 10 % to 36 %. The presence of a gap between pellets and rock at the roof does not influence significantly the results.

7 CONCLUSIONS

Finite element analyses have been carried out on several axisymmetric and full 3D models with variations of geometry, load conditions and constitutive models. After preliminary calibration through axisymmetric models, it has emerged that the assumption of an elasto-plastic model for foundation bed is necessary, as it is the part of the model where most deformations occur. Hence, the double-hardening Hardening Soil model was used as constitutive assumption for foundation material. In a selected number of analyses, a poroelastic model was used for saturated buffer, in order to simulate its expansion in a realistic manner. Remaining parts of the model have been modelled via the assumption of linear elasticity, which is rather rough for soils, but it is here made acceptable by introducing interface elements at the boundary of each soil cluster. Hence, it is expected that, due to material strength of backfill and buffer blocks, failure occurs at the contact surface rather than within the elements.

Amongst the several aspect considered throughout axisymmetric and 3D analyses, it appears that over-excavation, the presence of a roof gap and of a chamfer to ease the deposition procedure are not influencing the performance of buffer-backfill system. However, considering the variability that the section can have in reality due to excavation technique and the increased size of chamfer section, their influence will be considered in a further series of parametric studies, which will be documented in a separate report.

For present calculations the material assumed for foundation bed is 30/70 mixture of crushed rock and bentonite, but it is possible that, to fulfil the requirement of low permeability, the mixture will be replaced by bentonite granules. In the light of the obtained results, the expected heave should still be within an acceptable range, but further analyses should be performed once the final material has been selected.

The major uncertainties of numerical analysis are concentrated in mechanical properties of interfaces, in particular those between the blocks in deposition tunnel. Unless more precise information is obtained in future from experimental results, it to be envisaged a parametric study involving at least the mechanical properties of block-block and buffer-rock interfaces.

Although in Section 0 it is argued that the deformation of the system is not affected by block assembly, not having predefined routes for flow channels might increase the durability of the system reducing the risk of erosion due to fluid transport through the gaps.

Further studies are necessary to verify if the metal canister undergoes excessive displacement during buffer saturation process, although it seems to be unlikely because of the concentration of displacements in the upper part of buffer material.

In conclusion, from numerical analyses performed it results that the analysed solutions are compatible with the requirements of limited loss of density in buffer material, for a range of swelling pressure between 7 MPa and 15 MPa.

REFERENCES

Börgesson L. & Hernelind J. (2009). Mechanical interaction buffer/backfill. Finite element calculations of the upward swelling of the buffer against both dry and saturated backfill., Report R-09-42, SKB.
http://www.skb.se/upload/publications/pdf/R-09-42webb.pdf

Hansen J., Korkiala-Tanttu L., Keshi-Kuha E. & P. K. (2009). Deposition Tunnel Backfill Design for a KBS-3V repository, Report 2009-129, Posiva Oy.
http://www.posiva.fi/files/1242/WR_2009-129web.pdf

Johannesson L.-E., Sandén T., Dueck A. & Ohlsson L. (2010). Characterization of a backfill candidate material, IBECO-RWC-BF. Baclo Projekt − Phase 3. Laboratory tests, Report SKB R-10-44, Clay Technology AB.
http://www.skb.se/upload/publications/pdf/R-10-44webb.pdf

Juvankoski M. (2009). Description of Basic Design for Buffer, Report 2009-131.
http://www.posiva.fi/files/1277/WR_2009-131_rev2.web.pdf

Karnland O. (2010). Chemical and mineralogical characterization of the bentonite buffer for the acceptance control procedure in a KBS-3 repository, SKB.
http://www.skb.se/upload/publications/pdf/TR-10-60webb.pdf

Karnland O., Olsson S. & Nilsson U. (2006). Chemical and mineralogical characterization of the bentonite buffer for the acceptance control procedure in a KBS-3 repository, SKB. http://www.skb.se/upload/publications/pdf/TR-06-30webb.pdf

Korkiala-Tanttu L. (2009). Finite Element modelling of deformation of unsaturated backfill due to swelling of the buffer, Report 2008-88.
http://www.posiva.fi/files/1082/WR_2008-88web.pdf

Korkiala-Tanttu L., Keto P., Kuula-Väisänen P., Vuorimies N. & Adam D. (2007). Packfill-Development of in situ Compaction. Test Report for Field Tests November 2005, Report 2007-75. http://www.posiva.fi/files/827/WR_2007-75_web.pdf

Kuula-Väisänen P., Leppänen M. & Kolisoja P. (2009). BACLO - Processes during saturation of the block backfill. Mechanical properties and saturation of the block backfill. , Tampere University of Technology, Earth and Foundation Structures.

Ohde J. (1939). Zur Theorie der Druckverteilung im Baugrund. Der Bauingenieur, Berlin, Vol. 20: 451-459.

APPENDIX 1

In order to calibrate the finite element model and to gain insight in the basic behaviour of the buffer-backfill system, several preliminary axisymmetric calculations have been performed. For the sake of readability, results obtained are not included in the main section of this document, although vertical heave after saturation has been reported in Table 6. With respect to mesh geometry, in these analyses a slightly simpler mesh than that employed in Case AX01 has been chosen. The purpose is to reduce calculation time in the light of the deformation mechanism obtained from AX01, which shows very little displacements below canister top level. The geometry for preliminary analyses is shown below (Figure 1). Calculation procedure and load application/removal to simulate the swelling is identical to that illustrated in Section 4.4.
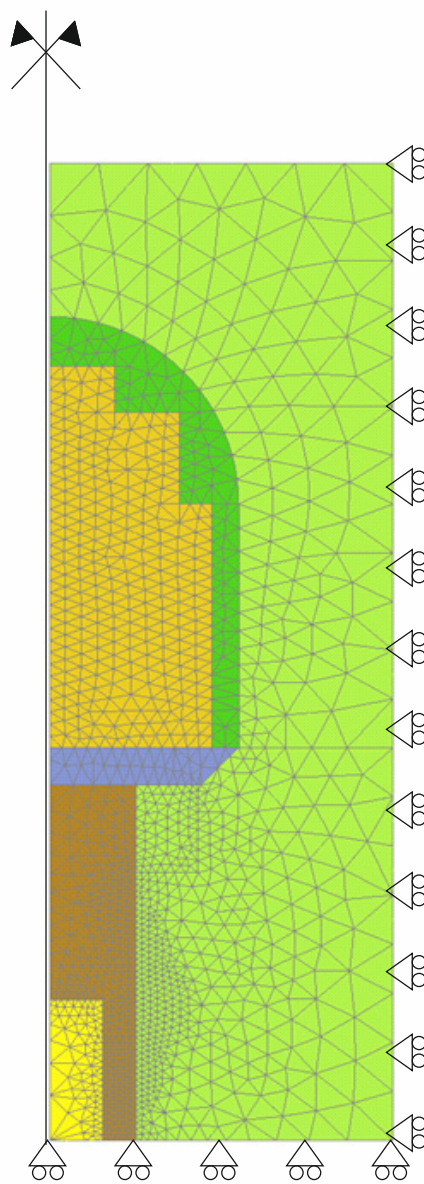

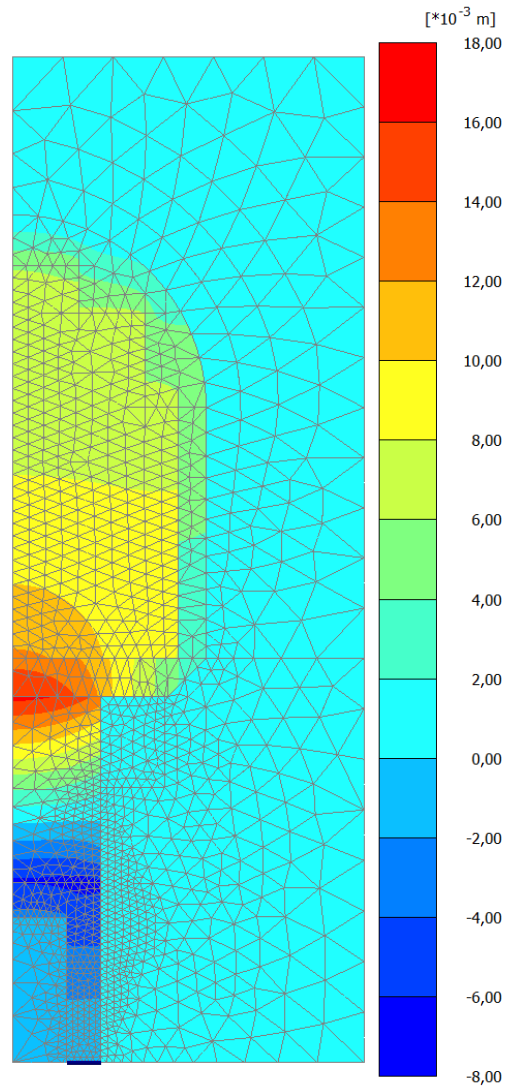***Figure 1.*** *Simplified model for preliminary axisymmetric calculations.*

Case AX02

Figure 2. *Vertical displacements.*

In this analysis all constitutive models are linear elastic, with linear elastic-perfectly plastic interface behaviour. Maximum vertical displacement value reached after free expansion of the buffer is 17 mm, reached at its top surface (Figure 2). The assumption of linear elasticity is not realistic especially for foundation bed, which is subjected to heavy shear and volumetric hardening.
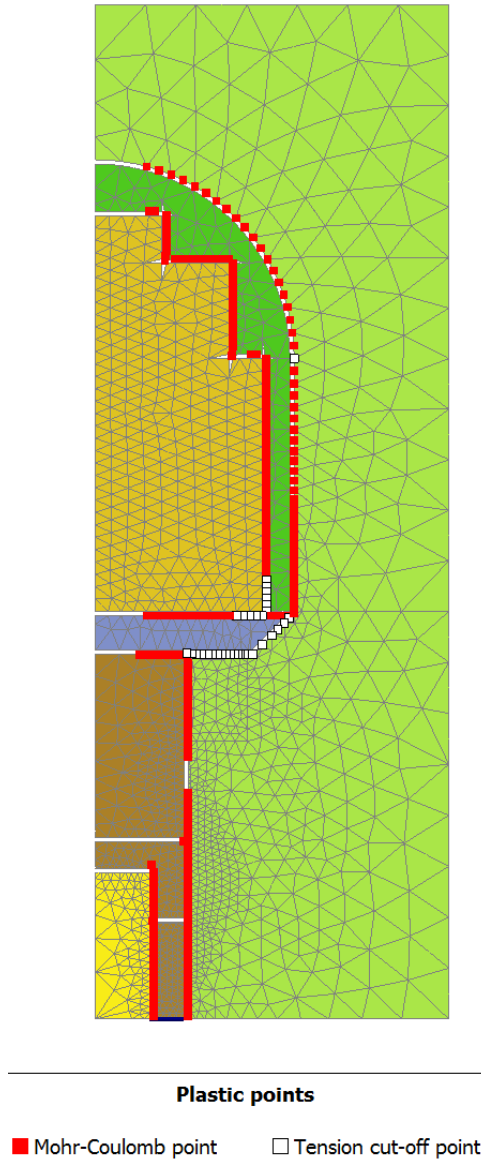
Plastic points

■ Mohr-Coulomb point   □ Tension cut-off point

Figure 3. *Plastic points after expansion.*

Figure 3 shows the distribution of plasticized points after expansion. It can be appreciated how the assumption of linear elasticity for every cluster implies a wide propagation of failure points, both for violation of Mohr-Coulomb failure criterion and for tensile failure. Obviously, all failure points are located in the interfaces, for which an elastic-perfectly plastic Mohr-Coulomb failure criterion has been chosen.

Case AX03
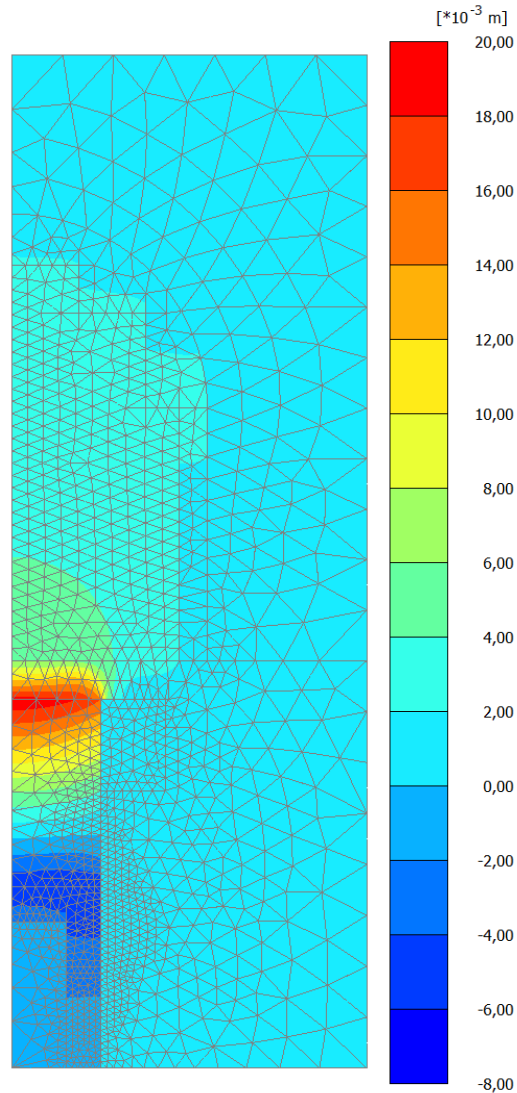

Figure 4. *Vertical displacements.*

In AX03 Hardening Soil model was used for foundation bed. Maximum vertical displacement is 20 mm (Figure 4). Due to hardening behaviour of foundation bed (for which the Hardening Soil model has been used in this case), deformations are concentrated in the central region whereas in previous case AX02 deformations can be observed in a wider region.
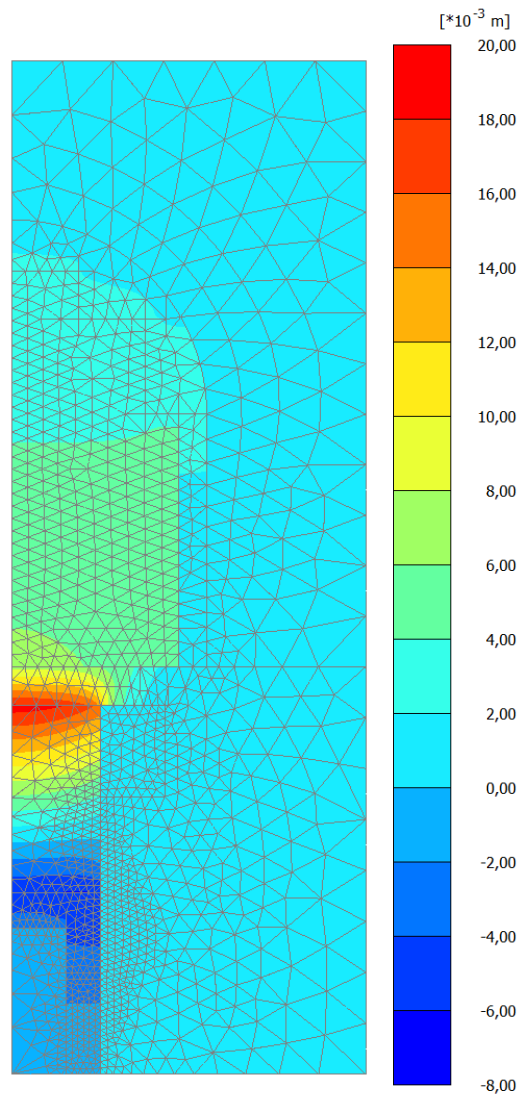
Case AX04

Figure 5. *Vertical displacements.*

In case AX04 it is assumed that bentonite pellets are used as foundation bed instead of 30/70 mixture. The effect is an increase of vertical displacements, to a maximum value of 19 mm. Distribution of vertical displacements is shown in Figure 5.

Case AX05
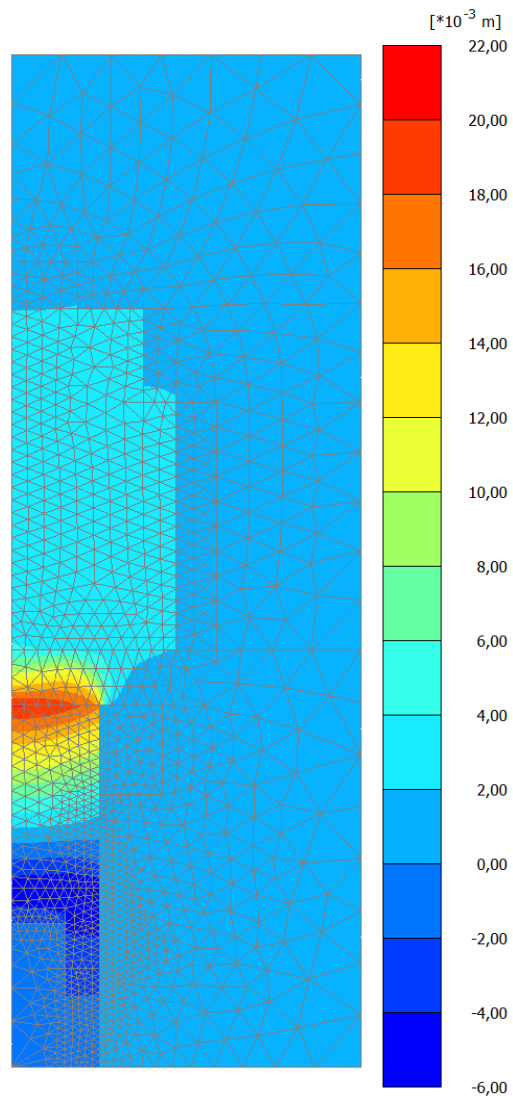
Figure 6. Vertical displacements.

In analysis AX05 it is assumed an over-excavation of 36 %, versus a standard value of 20 %. The thickness of pellet and foundation bed cluster is increased accordingly, and the effect is an increase of maximum vertical displacement to 20.3 mm (Figure 6).

Case AX06
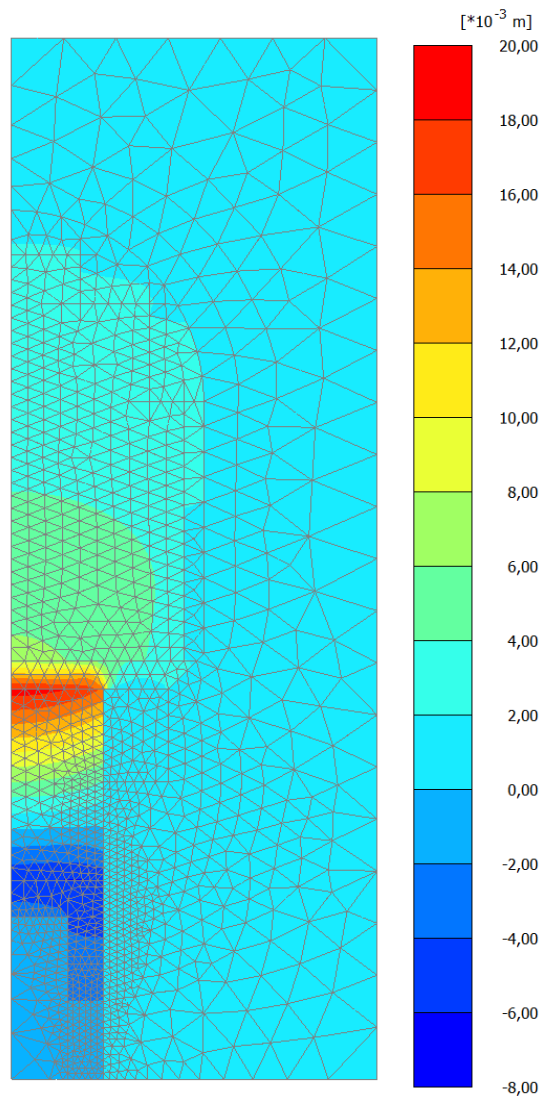
Figure 7. Vertical displacements.

In analysis AX06 whose results are shown in Figure 7, it is assumed an over-excavation of 10 %, versus a standard value of 20 %. The lower thickness of pellet and foundation bed cluster determines a vertical displacement of 19 mm, smaller than in standard case.

Case AX07
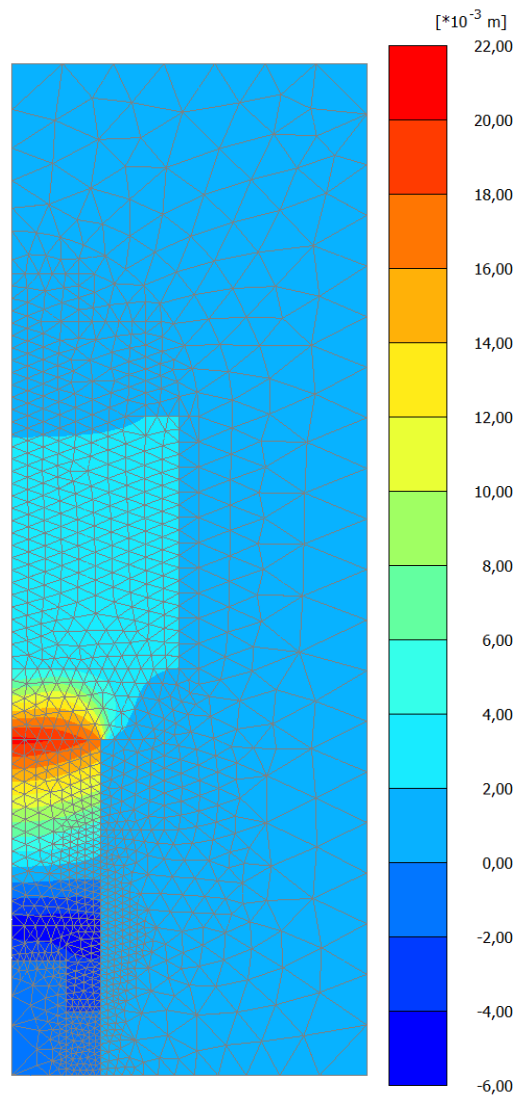
Figure 8. *Vertical displacements.*

Case AX07 includes 20 % over-excavation with increased floor thickness (550 mm). The maximum vertical displacement is 21 mm (Figure 8).

Case AX08
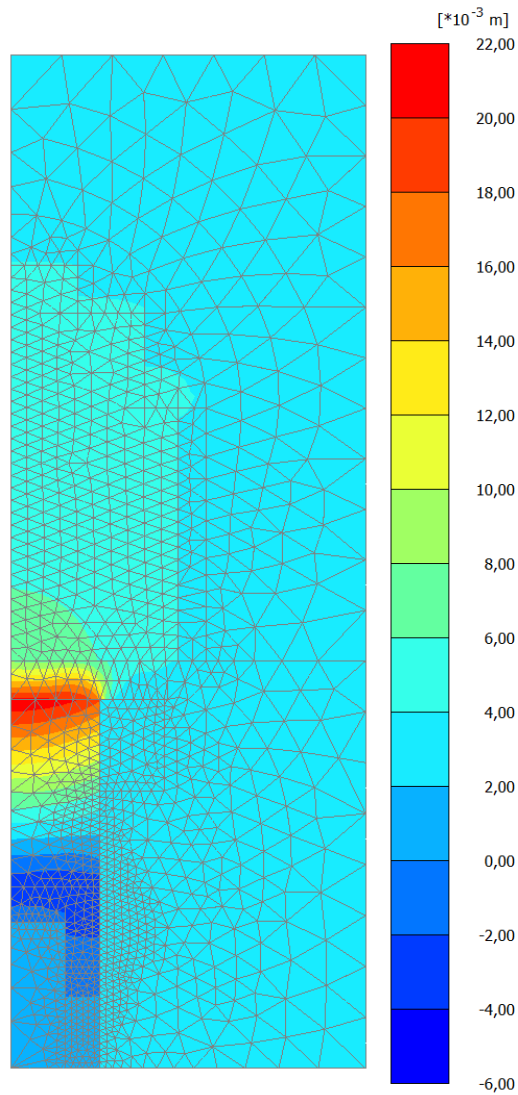
Figure 9. *Vertical displacements.*

In case AX08 a gap between pellets and roof is simulated by reducing to zero the corresponding interface stiffness. The effect is a maximum vertical displacement of 20.5 mm (Figure 9), thus exceeding by 0.5 mm the heave of case AX03. It is worth noting that the maximum vertical displacement at the roof is less than 10 mm, thus confirming that a gap of 10m or more in reality will not be sealed subsequently to buffer expansion.

Case AX09

Figure 10. *(Left) FE mesh with cylindrical chamfer (Right) Vertical displacements.*

A cylindrical region at the intersection between buffer and foundation bed is taken into account (Figure 10, Left). The region is filled with the same material used for foundation bed, and its influence on vertical displacement is very limited as it implies a maximum heave of 19.8 mm (Figure 10, Right) versus the 19 mm obtained in case AX03.

APPENDIX 2

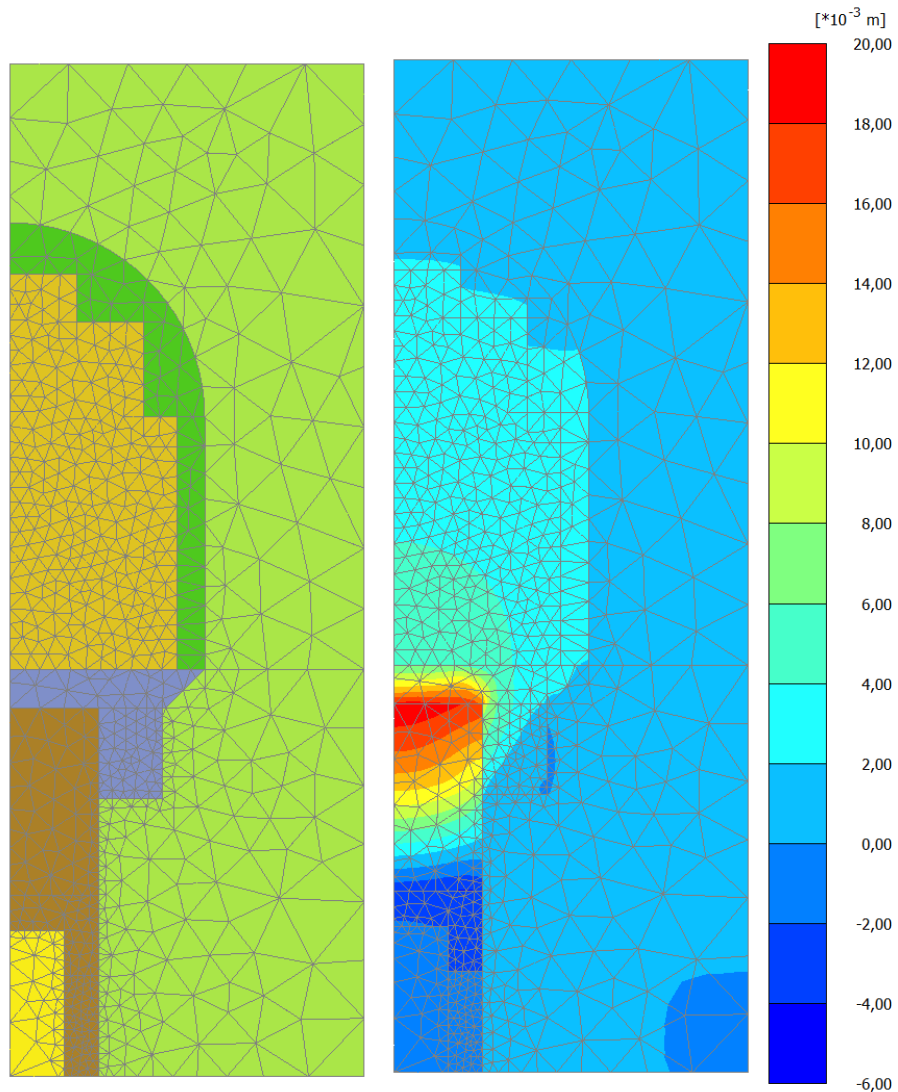Material parameters have been selected following the decisions taken in the first meeting held in Helsinki on 25th of November 2010, on the basis of previous publications and the experience gathered since the beginning of the project. In this Section are indicated the relevant documents used for parameters' identification.

Host rock   Assumed as mechanical boundary of the model, it is considered as rigid compared to bentonite blocks and pellets. In all analyses its stiffness was taken as high as 10 GPa.

Foundation bed   Strength parameters for Hardening Soil model have been determined according to triaxial tests reported in Appendix 16 of Korkiala-Tanttu *et al.* (2007) and shown in Figure 1. Instead of the suggested values of friction angle of 17.8° and effective cohesion as high as 102.2 kPa, considering the frictional nature of the mixture rather than its cohesive behaviour, it was decided to assume c'=60 kPa and φ'=24°.
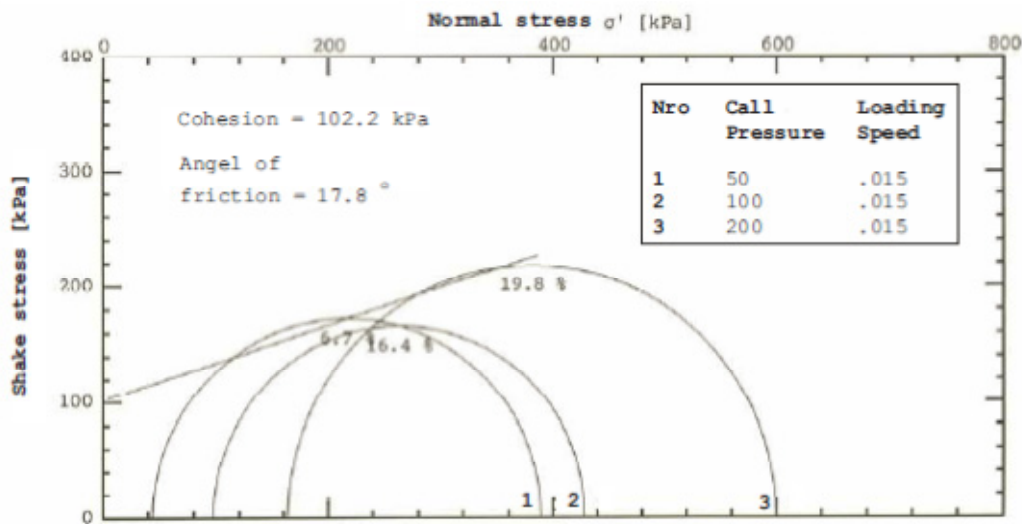
Figure 1. *Triaxial test results, Mohr circles. After Korkiala-Tanttu et al. (2007).*

Stiffness parameter E_{50}^{ref} for Hardening Soil model has been identified as indicated in Figure 2, as the secant modulus in correspondence of a stress deviator of 50 % of the ultimate one. E_{ur}^{ref} has been identified by means of the correlation $E_{ur}^{ref} \approx E_{50}^{ref}$ and $E_{oed}^{ref} \approx 3 \cdot E_{50}^{ref}$, thus obtaining:

$$E_{50}^{ref} = 9 \text{ MPa}; \qquad E_{ur}^{ref} = 27 \text{ MPa}; \qquad E_{oed}^{ref} = 9 \text{ Mpa}$$

The exponent m has been set to m = 0.7, typical for a mixture granular-fine grained soil, and Poisson's ratio ν'=0.2.
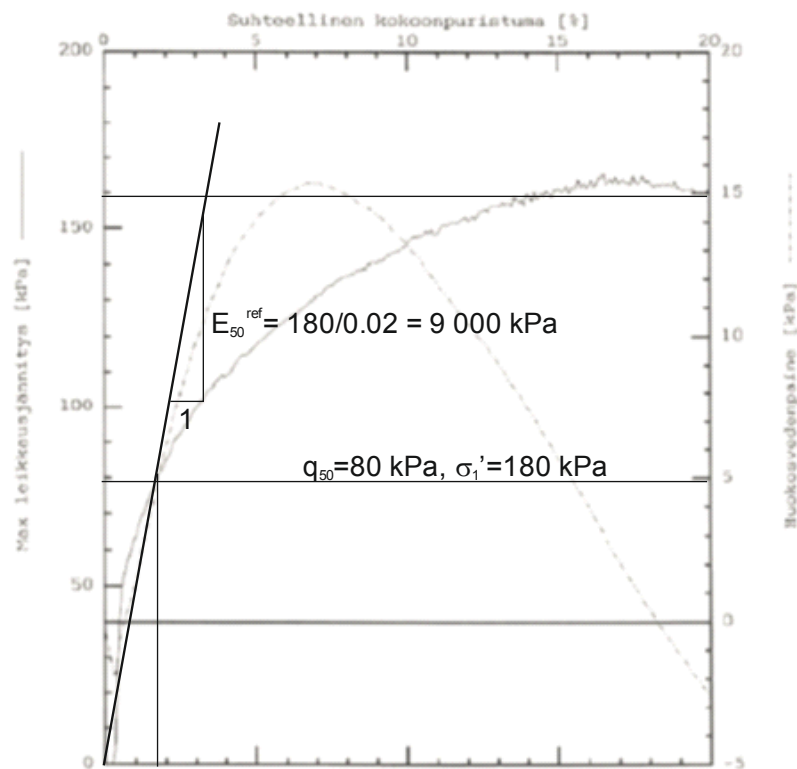
Figure 2. *Determination of E_{50}^{ref} from triaxial test results after Korkiala-Tanttu et al. (2007): stress deviator versus axial strain plot, cell pressure = 100 kPa.*

Bentonite pellets   Hardening Soil parameters used in preliminary analyses have been identified from test data reported in Johannesson *et al.* (2010), (E'=20 MPa, ν=0.12), and the final set of elastic parameters has been chosen as in Korkiala-Tanttu (2009), i.e. E'=20 MPa, ν'=0.12.

Blocks   Linear elastic as in parameters have been assumed as in Johannesson *et al.* (2010) (E'=264 MPa, ν=0.17)

Buffer   Linear elastic with E'=300 MPa and ν=0.28 (Korkiala-Tanttu 2009) and logarithmic stiffness with material data from Börgesson & Hernelind (2009) (κ=0.21, ν=0.4)

LIST OF REPORTS

POSIVA-REPORTS 2012

POSIVA 2012-01   Monitoring at Olkiluoto – a Programme for the Period Before
                 Repository Operation
                 Posiva Oy
                 ISBN 978-951-652-182-7

POSIVA 2012-02   Microstructure, Porosity and Mineralogy Around Fractures in Olkiluoto
                 Bedrock
                 Jukka Kuva (ed.), Markko Myllys, Jussi Timonen,
                 University of Jyväskylä
                 Maarit Kelokaski, Marja Siitari-Kauppi, Jussi Ikonen,
                 University of Helsinki
                 Antero Lindberg, Geological Survey of Finland
                 Ismo Aaltonen, Posiva Oy
                 ISBN 978-951-652-183-4

POSIVA 2012-03   Safety Case for the Disposal of Spent Nuclear Fuel at Olkiluoto -
                 Design Basis 2012
                 Posiva Oy
                 ISBN 978-951-652-184-1

POSIVA 2012-04   Safety Case for the Disposal of Spent Nuclear Fuel at Olkiluoto -
                 Performance Assessment 2012
                 Posiva Oy
                 ISBN 978-951-652-185-8

POSIVA 2012-05   Safety Case for the Disposal of Spent Nuclear Fuel at Olkiluoto -
                 Description of the Disposal System 2012
                 Posiva Oy
                 ISBN 978-951-652-186-5

POSIVA 2012-06   Olkiluoto Biosphere Description 2012
                 Posiva Oy
                 ISBN 978-951-652-187-2

POSIVA 2012-07   Safety Case for the Disposal of Spent Nuclear Fuel at Olkiluoto -
                 Features, Events and Processes 2012
                 Posiva Oy
                 ISBN 978-951-652-188-9

POSIVA 2012-08   Safety Case for the Disposal of Spent Nuclear Fuel at Olkiluoto -
                 Formulation of Radionuclide Release Scenarios 2012
                 Posiva Oy
                 ISBN 978-951-652-189-6

POSIVA 2012-09   Safety Case for the Disposal of Spent Nuclear Fuel at Olkiluoto - Assessment of Radionuclide Release Scenarios for the Repository System 2012
Posiva Oy
ISBN 978-951-652-190-2

POSIVA 2012-10   Safety case for the Spent Nuclear Fuel Disposal at Olkiluoto - Biosphere Assessment BSA-2012
Posiva Oy
ISBN 978-951-652-191-9

POSIVA 2012-11   Safety Case for the Disposal of Spent Nuclear Fuel at Olkiluoto - Complementary Considerations 2012
Posiva Oy
ISBN 978-951-652-192-6

POSIVA 2012-12   Safety Case for the Disposal of Spent Nuclear Fuel at Olkiluoto - Synthesis 2012
Posiva Oy
ISBN 978-951-652-193-3

POSIVA 2012-13   Canister Design 2012
Heikki Raiko, VTT
ISBN 978-951-652-194-0

POSIVA 2012-14   Buffer Design 2012
Markku Juvankoski, VTT
ISBN 978-951-652-195-7

POSIVA 2012-15   Backfill Design 2012
Posiva Oy
ISBN 978-951-652-196-4

POSIVA 2012-16   Canister Production Line 2012 – Design, Production and Initial State of the Canister
Heikki Raiko (ed.), VTT
Barbara Pastina, Saanio & Riekkola Oy
Tiina Jalonen, Leena Nolvi, Jorma Pitkänen & Timo Salonen, Posiva Oy
ISBN 978-951-652-197-1

POSIVA 2012-17   Buffer Production Line 2012 – Design, Production, and Initial State of the Buffer
Markku Juvankoski, Kari Ikonen, VTT
Tiina Jalonen, Posiva Oy
ISBN 978-951-652-198-8

POSIVA 2012-18   Backfill Production Line 2012 - Design, Production and Initial State of the Deposition Tunnel Backfill and Plug
Paula Keto (ed.), Md. Mamunul Hassan, Petriikka Karttunen,
Leena Kiviranta, Sirpa Kumpulainen, B+Tech Oy

Leena Korkiala-Tanttu, Aalto University
Ville Koskinen, Fortum Oyj
Tiina Jalonen, Petri Koho, Posiva Oy
Ursula Sievänen, Saanio & Riekkola Oy
ISBN 978-951-652-199-5

POSIVA 2012-19   Closure Production Line 2012 - Design, Production and Initial State of Underground Disposal Facility Closure
Ursula Sievänen, Taina H. Karvonen, Saanio & Riekkola Oy
David Dixon, AECL
Johanna Hansen, Tiina Jalonen, Posiva Oy
ISBN 978-951-652-200-8

POSIVA 2012-20   Representing Solute Transport Through the Multi-Barrier Disposal System by Simplified Concepts
Antti Poteri. Henrik Nordman, Veli-Matti Pulkkanen, VTT
Aimo Hautojärvi, Posiva Oy
Pekka Kekäläinen, University of Jyväskylä, Deparment of Physics
ISBN 978-951-652-201-5

POSIVA 2012-21   Layout Determining Features, their Influence Zones and Respect Distances at the Olkiluoto Site
*Tuomas Pere (*ed.), *Susanna Aro, Jussi Mattila,* Posiva Oy
Henry Ahokas & Tiina Vaittinen, Pöyry Finland Oy
Liisa Wikström, Svensk Kärnbränslehantering AB
ISBN 978-951-652-202-2

POSIVA 2012-22   Underground Openings Production Line 2012 – Design, Production and Initial State of the Underground Openings
Posiva Oy
ISBN 978-951-652-203-9

POSIVA 2012-23   Site Engineering Report
ISBN 978-951-652-204-6

POSIVA 2012-24   Rock Suitability Classification, RSC-2012
Tim McEwen (ed.), McEwen Consulting
Susanna Aro, Paula Kosunen, Jussi Mattila, Tuomas Pere, Posiva Oy
Asko Käpyaho, Geological Survey of Finland
Pirjo Hellä, Saanio & Riekkola Oy
ISBN 978-951-652-205-3

POSIVA 2012-25   2D and 3D Finite Element Analysis of Buffer-Backfill Interaction
Martino Leoni, Wesi Geotecnica Srl
ISBN 978-951-652-206-0